

Kinematics and geochronology of the Lancang metamorphic complex: Implications for the evolution of the Paleo-Tethys region

Ya Cui¹, Yang Wang^{1,2,†}, Renjie Zhou³, Jeremy Rimando⁴, Xin Qian^{1,2}, Yipeng Zhang^{1,2,†}, and Yuejun Wang^{1,2}

¹Guangdong Provincial Key Laboratory of Geodynamics and Geohazards, School of Earth Sciences and Engineering, Sun Yat-sen University, Guangzhou 5100275, China

²Southern Marine Science and Engineering Guangdong Laboratory, Zhuhai 519082, China

³School of Earth and Environmental Sciences, The University of Queensland, St. Lucia Queensland 4072, Australia

⁴School of Earth, Environment & Society, McMaster University, Hamilton, Ontario L8S 4K1, Canada

ABSTRACT


The Lancang metamorphic complex is a key component of the Three River Tethys Orogen in the SE Tibetan Plateau, with typical rock assemblages and deformation fabrics recording the subduction of the Paleo-Tethys Ocean and subsequent continental collision. In this study, we present new petrographic and structural observations, together with zircon U-Pb and mica ⁴⁰Ar/³⁹Ar geochronologic data, to reveal the deformation and kinematics of the Lancang metamorphic complex, thus providing insights into the Permian–Triassic evolution of the eastern Paleo-Tethys domain. The subduction of the Paleo-Tethys Ocean and subsequent collision resulted in a range of structural features, including penetrative regional foliations, thrusts, asymmetric folds at various scales, and ductile deformation fabrics such as asymmetric boudins and porphyroclasts. Zircon U-Pb dating of foliated gabbro and ⁴⁰Ar/³⁹Ar dating of mica schist and mylonite, which preserve shortening fabrics, suggest that the Paleo-Tethys Ocean was subducted during the Late Carboniferous to Permian–Early Triassic, and the collision of the Baoshan and Simao blocks mainly occurred during ca. 237–230 Ma in the SE Tibetan Plateau. Regional deformation likely shifted from shortening to extension ca. 230 Ma, as reflected by post-collision high-K calc-alkaline magmatism. Our results document regional structural patterns and place timing constraints on the evolution of the Paleo-Tethys Ocean.

1. INTRODUCTION

The Paleo-Tethys Ocean existed from the Paleozoic to Late Triassic (e.g., Wang et al., 2010, 2018b, 2019; Metcalfe, 1996, 2013, 2021; Deng et al., 2018; Hu et al., 2020, 2022), and the geologic records for the Paleo-Tethys tectonic belt extend from the European Alps, through Southwest China, to Peninsular Malaysia in Southeast Asia. They document the opening and demise of the ocean and the accretion and aggregation of various blocks on the Asian continent (e.g., Wang et al., 2010, 2018b; Deng et al., 2018; Metcalfe, 2013, 2021; Morley, 2018; Hu et al., 2020, 2022). The Three River orogenic belt in the SE Tibetan Plateau is a critical component of the eastern Paleo-Tethys domain, which straddles the area from the Eastern Himalayan Syntaxis to the Indochina Peninsula (Fig. 1A; e.g., Helmcke, 1985; Zhong, 1998; Peng et al., 2008, 2013; Jian et al., 2009a, 2009b; Hennig et al., 2009; Wang et al., 2010; Fan et al., 2015; Xu et al., 2015). Several major tectonic belts—including the Ailaoshan–Songma, Lancangjiang, and Nujiang belts—preserve the geologic record of multiple island-ocean paleogeographic patterns and oceanic subduction and collision (Fig. 1A; e.g., Hesse et al., 2007; Jian et al., 2009b; Wang et al., 2019; Li et al., 2021). Diverse rock assemblages outcrop along these belts, including ophiolite suites, metamorphic rocks of various grades, volcanics, and S-, I-, and A-type pre-/syn-/post-collisional igneous rocks (e.g., Zhao et al., 1994; Zhong, 1998; Jian et al., 2009b; Wang et al., 2010; Fan et al., 2015; Deng et al., 2018). These belts also consist of various tectonites, such as schist, mylonite, and gneiss, with abundant deformation fabrics that document different evolutionary stages of the Paleo-Tethys Ocean and its branch oceans (e.g., Zhao et al., 1994; Zhong, 1998; Bi et al., 2018; Zhang et al., 2017; Wang et al., 2017, 2020b, 2022).

The Lancangjiang tectonic belt trends N–S within the Indochina Peninsula, separating the Baoshan–Sibumasu and Simao–Indochina blocks (Fig. 1B; Zhong, 1998; Metcalfe, 2013; Peng et al., 2008), and is the most intricate tectonic complex of the Three River orogenic belt. The main tectonic elements within the belt comprise the Changning–Menglian suture zone, Lancang metamorphic complex, Lincang igneous belt, and Banpo–Jinghong back-arc system (Fig. 1B). The Changning–Menglian suture zone extends from SW Yunnan, China, across NW Laos, and links to the Inthanon–Bentong–Raub suture zone in NW Thailand (Fig. 1B; Wang et al., 2018b; Metcalfe, 2013, 2021). Remnants of the Paleo-Tethys Ocean along the suture zone include an ophiolite mélange, a radiolarian siliceous–argillaceous sequence, deep-sea mudstones with radiolarians, metamorphic rocks, and related igneous rocks (e.g., Zhong, 1998; Zhang et al., 2008; Metcalfe, 2013; Mo et al., 1998; Peng et al., 2008, 2013; Hennig et al., 2009). These rocks yield zircon U-Pb ages of 385–267 Ma, which are thought to be related to the spreading and subduction of the Paleo-Tethys Ocean (e.g., Feng and Liu, 1993; Duan et al., 2006; Jian et al., 2009a; Deng et al., 2018; Wang et al., 2016b, 2018b).

The Lancang metamorphic complex is sandwiched between the Changning–Menglian suture and Lincang igneous belt and exhibits spatially diverse along-strike deformation and metamorphism (Fig. 1B; Zhao et al., 1994; Zhong, 1998; Fan et al., 2015; Zhai et al., 2019). High-pressure/low-temperature metamorphic rocks, including metasedimentary clastic rocks, greenschists, blueschists, and high- to ultrahigh-pressure metamorphic rocks, yield ⁴⁰Ar/³⁹Ar ages of 246–227 Ma, which record the regional metamorphism related to oceanic subduction and continental collision (e.g., Fan et al., 2015; Wang et al., 2014b, 2019, 2020a, 2021). The

Yang Wang  <https://orcid.org/0000-0001-7384-5571>

[†]Yang Wang, wangyang26@mail.sysu.edu.cn; Yipeng Zhang, zhangyp45@mail3.sysu.edu.cn

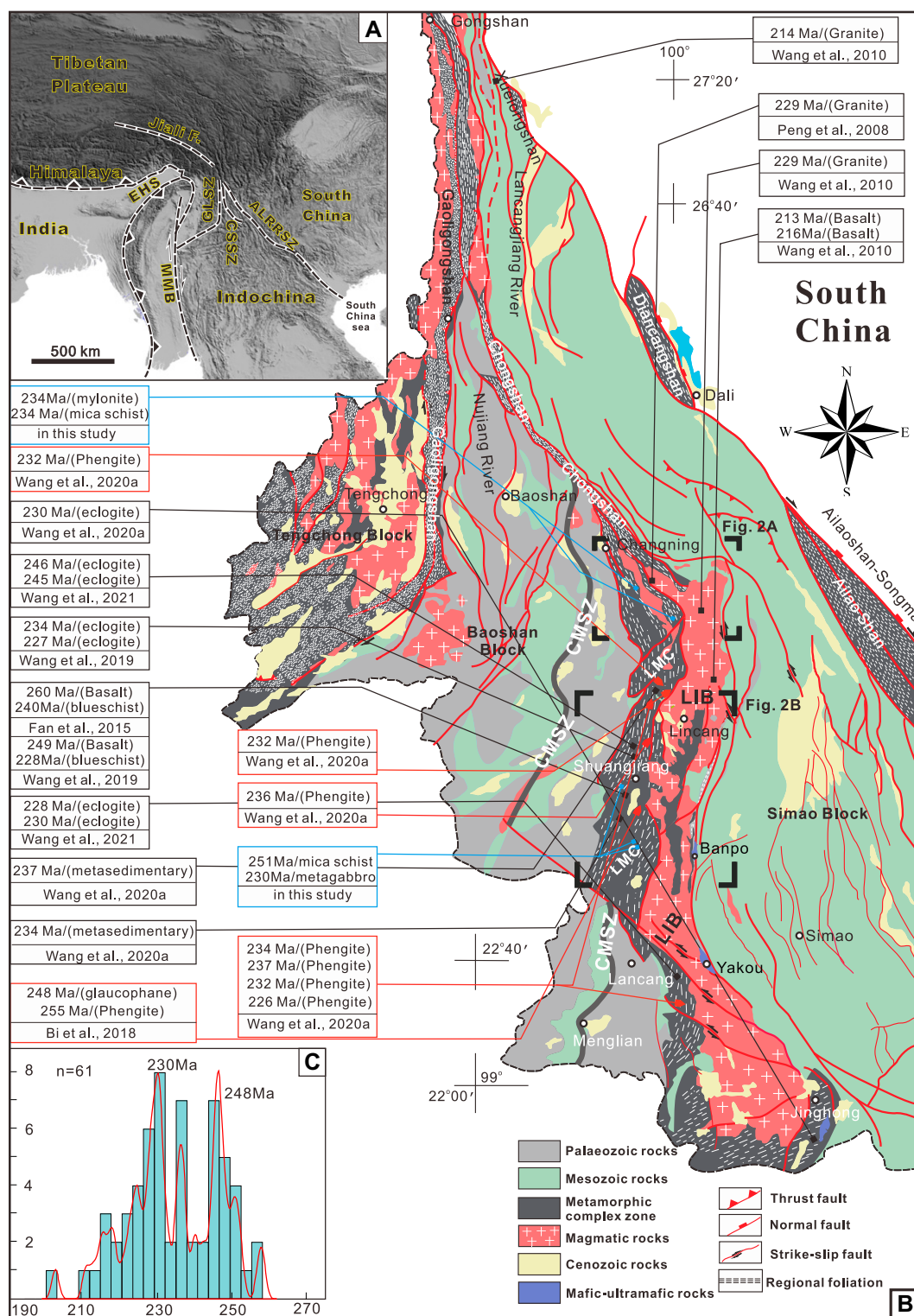


Figure 1. (A) Simplified tectonic framework of the Tibetan Plateau and adjacent regions. **(B)** Geological map of south-western Yunnan (modified from Wang et al., 2022) and chronological data from this and previous studies. The red and black boxes indicate $^{40}\text{Ar}/^{39}\text{Ar}$ and zircon U-Pb data from previous studies, respectively; the blue boxes indicate data from this study. **(C)** Spectrum of ages for Lincang granite (Deng et al., 2018, and references therein). ALRRSZ—Ailaoshan–Red River shear zone; CMSZ—Changning–Menglian suture zone; CSSZ—Chongshan shear zone; EHS—eastern Himalayan syntaxis; F.—formation; GLSZ—Gaoligong shear zone; LIB—Lincang igneous belt; LMC—Lancang metamorphic complex; MMB—Mogok meta-morphic belt.

Lincang igneous belt is inferred to be connected to the Sukhothai arc and the Triassic giant igneous belt in East Malaysia and displays multiple stages of emplacement in different tectonic settings (Fig. 1C; e.g., Peng et al., 2008; Wang et al., 2010, 2018b; Fan et al., 2015; Deng et al.,

2018; Cong et al., 2020). Existing geochronologic and geochemistry data collected from the Lincang granitoids reveal three main magmatic episodes that are correlated with oceanic subduction prior to ca. 252 Ma, followed by syn-collisional magmatism from 250 Ma to 230 Ma,

and a post-collisional phase from 230 Ma to 200 Ma (e.g., Peng et al., 2013; Fan et al., 2009; Hennig et al., 2009; Jian et al., 2009a, 2009b; Kong et al., 2012; Dong et al., 2013; Deng et al., 2018). The Banpo–Jinghong mafic-ultramafic complexes are situated on the western margin

of the Simao block and have zircon U-Pb ages of 313–281 Ma (e.g., Hennig et al., 2009; Jian et al., 2009b; Li et al., 2012; Zhai et al., 2019), which represent a back-arc basin related to the main Paleo-Tethys Ocean (e.g., Li et al., 2012; Wang et al., 2018b; Zhai et al., 2019).

Previous studies have advanced our understanding of magmatism and metamorphism along the Lancangjiang tectonic belt, but interpretations regarding the evolution of the Paleo-Tethys remain controversial. Little is known about the kinematics, deformation patterns, and associated age constraints. In this study, we target the Lancang metamorphic complex with field-based structural and kinematic analysis. Our geological observations, together with new and published geochronologic results, constrain the timing of metamorphism and deformation in the Mesozoic and provide new insights into the evolutionary history and geodynamics of the eastern Paleo-Tethys domain.

2. GEOLOGICAL SETTING

The Lancangjiang tectonic belt, located in the central part of the Indochina Peninsula, extends southward from the Eastern Himalayan Syntaxis to northern Thailand. There appear to be significant differences in the structural style and timing, from N to S, along the belt (Fig. 1A; e.g., BGMRY, 1990; Mo et al., 1998; Zhong, 1998; Li et al., 2012; Peng et al., 2013; Fan et al., 2015). Three tectonic units are identified from west to east: the Baoshan-Sibumasu block, the Lancangjiang tectonic belt, and the Simao-Indochina block (e.g., Fang et al., 1994; Peng et al., 2008, 2013; Fan et al., 2015; Zhai et al., 2019; Wang et al., 2020b). However, deformation during the Indosinian Orogeny and the Cenozoic juxtaposed units from these different tectonic provinces. Due to the lithological similarities and a sparsity of fossils in some units at the tectonic boundary, it can be difficult to attribute to which provinces a particular sedimentary unit may belong.

The Baoshan block is bordered by the Changning-Menglian suture zone to the east and by the Gaoligong shear zone to the west (Fig. 1B; Metcalfe, 2013). It is considered to be the northern part of the Sibumasu continental fragment and has stratigraphic and paleontological affinities to Gondwana (e.g., Fang et al., 1994; Feng, 2002; Metcalfe, 2013, 2021; Zhong, 1998). The oldest exposed strata in the Baoshan block belong to the Cambrian Gongyanghe Group, which comprises shallow metamorphic sandstone and quartz sandstone that correspond to the Neoproterozoic to Cambrian Chaung Magyi Group in Myanmar (e.g., Zhu et al., 2011; Morley, 2018). The Ordovician–Middle Triassic rock strata are

mainly composed of sedimentary neritic clastic rocks interbedded with mudstone and limestone shale. Due to the Indosinian Orogeny, there is barely a record of sediments from the Late Triassic to the Early Jurassic (e.g., BGMRY, 1990; Zhong, 1998). In the Middle Jurassic, continental molasse formations began to be deposited, which were mainly composed of purple-red coarse terrigenous clastic rocks interbedded with basic volcanic rocks. Multi-phase continental volcanics were formed in the Early Permian and Middle Jurassic (e.g., BGMRY, 1990; Zhong, 1998; Liao et al., 2013).

The Lancangjiang tectonic belt consists of the Changning-Menglian suture, Lancang metamorphic belt, Lancang igneous belt, and Banpo-Jinghong back-arc system. The Changning-Menglian suture zone is considered to be the remnant of the main Paleo-Tethys oceanic crust in SW China and is possibly connected to the Longmuco-Shuanghu suture zone in central Tibet, the Chiang Mai suture zone in Thailand, and the Bentong-Raub suture zone in Malaysia farther to the south (e.g., Peng et al., 2008, 2013; Wang et al., 2016b, 2018b; Zhai et al., 2019; Li et al., 2021; Fu et al., 2021; Wei et al., 2022). The suture zone consists of a complex assemblage of ophiolitic mélanges, rock units representing residual oceanic islands and seamounts, as well as Triassic high-pressure metamorphic rocks (blueschist and eclogite), which experienced diverse deformation and metamorphism (e.g., Zhao et al., 1994; Zhong, 1998; Jian et al., 2009a, 2009b; Nie et al., 2015; Sun et al., 2017, 2020; Li et al., 2017; Wang et al., 2019; Fu et al., 2021; Zhai et al., 2019). The Nantinghe-Manxin area ophiolites have given U-Pb ages of 470–439 Ma, which are related to the Proto-Tethyan Ocean (e.g., Yan et al., 2022; Wang et al., 2013, 2014a, 2016a, 2018a; Sun et al., 2017). Remnants of oceanic-island basalt volcanic edifices and fossiliferous seamount carbonates within the suture zone have an overall age range of Late Devonian to Late Permian (e.g., Metcalfe, 2013, 2021; Ito et al., 2020). The Niujingshan ophiolite was dated at 386 Ma (late Middle Devonian) and likely represents the initial spreading of the east Paleo-Tethys Ocean (e.g., Fang et al., 1994; Wang et al., 2018b). Supra-subduction zone ophiolites and normal mid-oceanic-ridge basalt (N-MORB) gabbros were dated at 272–264 Ma, which reflects the main subduction of the Paleo-Tethys Ocean in the Permian (e.g., Jian et al., 2009b; Wang et al., 2018b, 2019; Fu et al., 2021; Zhai et al., 2019).

The N–S–striking Lancang metamorphic complex extends discontinuously for more than 200 km along the Lancang River (e.g., Zhao et al., 1994; Zhong, 1998; Fan et al., 2015; Wang et al., 2017, 2020b; Bi et al., 2018). The

complex mainly includes the Xiaoheijiang greenschist-facies and Lancang metamorphic mélange rocks, which have undergone intense shortening deformation and ductile shearing and are overlain by an unconformity by the Upper Triassic–Lower Jurassic molasse deposits (e.g., Zhao et al., 1994; Zhong, 1998; Fan et al., 2015). The Xiaoheijiang rock units consist mainly of Carboniferous–Lower Triassic greenschist-facies quartz sandstone, quartz greywacke, and pelitic rocks, which contain minor volcanoclastic rocks (e.g., Zhao et al., 1994; Zhong, 1998; Fan et al., 2015; Bi et al., 2018). The Lancang metamorphic mélange rocks are dominated by mica schist, greenschist, and blueschist, with minor metamorphic volcanics and marble (e.g., Zhong, 1998; Fan et al., 2015). High-pressure metamorphic rocks yield Rb–Sr isochron ages of polysilicic muscovite of 260–240 Ma, and the blueschists give $^{40}\text{Ar}/^{39}\text{Ar}$ ages of 248–242 Ma (e.g., Zhao et al., 1994; Fan et al., 2015; Wang et al., 2018b). In addition, the deformation fabrics are well preserved in the Lancang metamorphic complex, and the $^{40}\text{Ar}/^{39}\text{Ar}$ plateau age of the mica schist is 248 Ma (Wang et al., 2022), which may approximate the timing of crustal shortening related to the subduction-collision stage of the Paleo-Tethys Ocean.

The Lancang igneous belt is mainly composed of Triassic granites and associated volcanic sequences and is one of the most remarkable geological features in SW Yunnan (Fig. 1B; e.g., Liu et al., 1989; Peng et al., 2008; Wang et al., 2012; Fan et al., 2015; Zhao et al., 2018; Zhai et al., 2019). It extends southward over 370 km and links to the Baimaxueshan granitoid batholiths in the north and the Sukhothai and East Malaysia granitoid batholiths in Southeast Asia (Fig. 1B; e.g., Jian et al., 2003, 2009a, 2009b; Fan et al., 2009, 2010; Dong et al., 2013; Wang et al., 2019). The Lancang-Sukhothai arc is bounded by the Changning-Menglian (Lancang metamorphic belt), Inthanon, and Bentong-Raub suture zones to the west, and by the Banpo-Jinghong-Nan-Uttaradit suture zone to the east (e.g., Ueno, 1999; Ueno and Hisada, 1999, 2001; Sone et al., 2012; Metcalfe, 2013, 2021; Morley, 2018). The arc is dominated by the thick volcanic sequences and A-, I-, or S-type batholiths (e.g., Wang et al., 2010, 2018b; Peng et al., 2013; Fan et al., 2015; Deng et al., 2014, 2018). It formed on the western margin of the Simao-Indochina block due to the eastward subduction of the Paleo-Tethys Ocean (e.g., Wang et al., 2018b; Zhai et al., 2019; Metcalfe, 2013, 2021) and was separated by back-arc spreading in the Late Carboniferous–Middle Permian and then accreted back onto the Simao-Indochina block by back-arc closure in the Triassic. These granitoids in the Lancang-Sukhothai

arc comprise a composite batholith, which is mainly composed of monzonitic biotite granite, K-feldspar granite, and granodiorite, and have yielded crystallization ages of 261–200 Ma (predominant ages cluster at 230–220 Ma) with a multi-stage emplacement history (e.g., Wang et al., 2010, 2018b; Peng et al., 2013; Fan et al., 2015; Deng et al., 2014, 2018). Previous studies show that the Late Permian–earliest Triassic granitoids within the Lincang–Sukhothai arc igneous belt are mainly high-K calc-alkaline series and I-type granites that have arc-island features (e.g., Chappell et al., 2012; Dong et al., 2013; Fan et al., 2015; Deng et al., 2018; Cong et al., 2020). The Early–Middle Triassic granitoid magmatism ranges from 250 Ma to 237 Ma and shows S- and I-type characteristics with various deformation or metamorphism, which indicates a syn-collisional setting (e.g., Zhu et al., 2011; Bi, 2014; Fan et al., 2015). In contrast, the Late Triassic granitoids from 235 Ma to 200 Ma exhibit high-K calc-alkaline and A-/S-type signatures that mainly reflect a post-collisional setting (e.g., Wang et al., 2010; Deng et al., 2018). Therefore, the Lincang–Sukhothai batholith mainly records three magmatic events related to the subduction, collision, and post-collision of the Paleo-Tethys Ocean (e.g., Wang et al., 2010, 2014a, 2018b; Deng et al., 2018; Hu et al., 2022). In addition, the volcanic sequence comprises the Mannguhai, Xiaodingxi, and Manghuihe formations with zircon U–Pb ages of 241–210 Ma, which form an angular unconformity with the overlying Late Triassic to Early Jurassic red foreland molasse of the Yiwanshui formation. These formations have been interpreted as a post-collision product (e.g., BGMRYP, 1990; Zhong, 1998; Feng, 2002; Peng et al., 2013; Wei et al., 2016).

The Banpo–Jinghong belt is represented by three mafic-ultramafic complexes in the Banpo, Yakou, and Jinghong areas; it extends southward and likely links to the Nan–Sa Kao back arc in Southeast Asia (e.g., Wang et al., 2018b; Metcalfe, 2013). The rock assemblage includes pyroxenite, gabbro, diorite, and basaltic andesite (e.g., Jian et al., 2009a; Li et al., 2012; Zhai et al., 2019), which exhibit zircon U–Pb ages of 313–281 Ma (e.g., Hennig et al., 2009; Jian et al., 2009b; Li et al., 2012; Zhai et al., 2019). The geochemical characteristics of the gabbros and basalts are similar to those of MORB, with the following isotopic geochemistry: $^{87}\text{Sr}/^{86}\text{Sr}(t)$ ratio (0.7045–0.7064), $\varepsilon_{\text{Nd}}(t)$ (+3.4 to +6.7), zircon $\varepsilon_{\text{Hf}}(t)$ (+12.4 to +14.3), and $\delta^{18}\text{O}$ (‰) (–5.5‰), which indicate that the Banpo–Jinghong basic rock belt may represent a back-arc basin related to the eastward subduction of the Paleo-Tethys Ocean (Li et al., 2012; Wang et al., 2018b; Zhai et al., 2019).

The Simao–Indochina block is bounded by the Lancangjiang tectonic belt to the west and the Ailaoshan–Red River shear zone to the east (Fig. 1B; Fan et al., 2010; Liu et al., 1989; Metcalfe, 1996, 2013; Zhong, 1998; Wang et al., 2020b, 2022). The Paleozoic metasedimentary rocks show similar lithologies to those of the Yangtze block to the east, with typical Cathaysia flora and fauna; the main metamorphic basement is represented by the Damenlong and Chongshan complexes, which are mainly composed of metavolcanics, siliciclastics, and marbles (e.g., Zhong, 1998; Akciz et al., 2008; Wang et al., 2010; Fan et al., 2010). The lower Paleozoic metasedimentary rocks are unconformably overlain by Middle Devonian–Permian conglomerates and siliciclastic rocks (e.g., BGMRYP, 1990; Zhong, 1998; Fan et al., 2010; Wang et al., 2010, 2019). Carboniferous–Permian strata are mainly composed of basic volcanic rock, shallow marine carbonate rock, and sandy argillaceous rocks (e.g., Feng, 2002; Metcalfe, 2013; Zhao et al., 2018). Records of Early Triassic sediments are hardly present in the Simao–Indochina block. Middle Triassic volcanic formations developed on both sides of the block (Lincang–Sukhothai granite on the western side, and Jinshajiang–Ailaoshan–Songma Middle Triassic volcanic rocks on the eastern side). The Middle and Upper Triassic rocks are mainly formed of stable platform sandy argillaceous carbonates. In the Late Triassic, the Indosinian Orogeny may have caused most of the area to be uplifted into a landmass, and only carbonates of offshore continental basin facies were deposited locally (e.g., BGMRYP, 1990; Zhong, 1998; Ueno and Hisada, 2001). After the Jurassic, a set of striking red continental deposits developed (e.g., BGMRYP, 1990; Zhong, 1998; Ueno and Hisada, 2001; Metcalfe, 2013).

3. STRATIGRAPHY AND DEFORMATION

The major stratigraphic units exposed along the Lancang metamorphic complex include the Proterozoic (Pt), Paleozoic (Pz, include Ordovician, Devonian, Carboniferous, and Permian), and Mesozoic (Mz, Triassic) strata, which experienced variable deformation and metamorphism (Figs. 2 and 3; BGMRYP, 1990).

In the Lancangjiang tectonic belt, the Proterozoic strata (Pt, including the Manlai and Huimin formations in the upper part of the Lancang Group; BGMRYP, 1990; Zhong, 1998) are well exposed and form a long and narrow greenschist–amphibole–facies metamorphic belt with intense deformation. This belt is mainly composed of quartz schist, mica schist, and granulite. At Location 1 (Fig. 2B), thin-to-thick mica schist

and slate are alternately exposed with penetrative foliations and cleavages (Fig. 4A). Several thrust faults and abundant asymmetric folds developed at this outcrop (Figs. 4A–4C). Most of the fault planes dip westward (243° – 268°), with a dip angle of 31° – 62° (Fig. 4A). They generally slide along the weak slate and form fault zones with various widths. Fault gouges are 10–15 cm thick with penetrative cleavages (Fig. 4A). The foliations and cleavages show characteristics of S–C fabrics (Fig. 4C). Quartz veins were deformed into asymmetric boudins due to ductile shearing. At various scales in the region, east-verging asymmetric folds indicate top-to-the-east thrusting (Fig. 4). At Location 2 (Fig. 2B), mica schists of the Proterozoic strata exhibit penetrative foliations and west-plunging lineations (Figs. 4D and 4F). The quartz veins were deformed into asymmetric porphyroclasts and boudins (Fig. 4E), indicating similar kinematics.

Paleozoic strata (Pz), as defined by the BGMRYP (1990), contain greenschist- to low-amphibolite-facies metamorphic rocks such as mica-quartz schist, mylonite, and gneiss. At Location 3 (Fig. 2A), mylonites of the Paleozoic strata exhibit penetrative foliations that dip steeply toward the west and form asymmetric folds (Fig. 5A). Kinematic indicators such as asymmetric calcite, quartz porphyroclasts, and asymmetric folds indicate top-to-the-east thrusting (Figs. 5A and 5F).

Ordovician strata mainly outcrop in the northern segment of the Lancang metamorphic complex (Fig. 2A). The Ordovician is dominated by metamorphosed sandstone, quartz schist, and mica schist, which preserve foliations, lineations, and ductile deformation fabrics that are indicative of crustal shortening. For example, at Location 4 (Fig. 2A), mica schists with pervasive foliations were well exposed and dip toward the NE to E (63° – 87°) with dip angles of 45° – 65° (Fig. 6A). The lineations observed on the foliations mostly plunge ENE (Fig. 6C). Asymmetric porphyroclasts, boudins, and S–C fabrics are well developed at the outcrop scale, which indicates top-to-the-west thrust shearing (Figs. 6B and 6D).

Devonian strata are mainly composed of carbonatite and argillaceous carbonatite rocks that are distributed in a N–S direction. The deformation is extensive and exposes regional penetrative foliations (Fig. 2B). A typical ramp-shaped flat structure is present at Location 5 along the Xiaohaijiang River (Figs. 2B, 3, and 7A), which is the typical deformation style of the Devonian strata. The dip angle of the thrust-fault plane is 56° at the lower part and gradually becomes gentler upward. Sub-horizontal or gently dipping slate is exposed in the footwall and plunges $\sim 5^{\circ}$ – 15° toward the W–NW (260° – 287° ; Fig. 7A). The

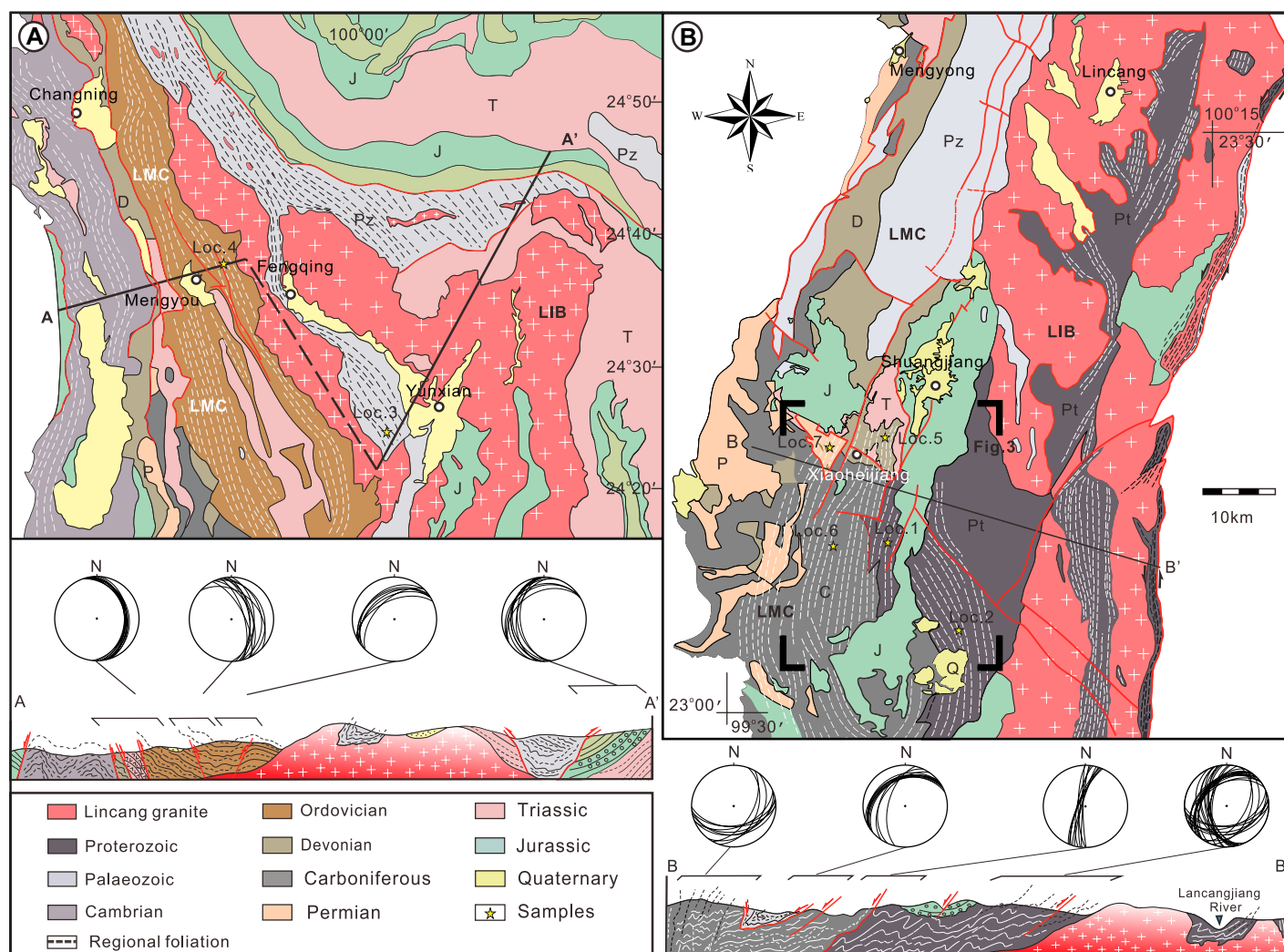


Figure 2. Geological map of the northern and central parts of the Lancang metamorphic complex and adjacent regions (BGMRYP, 1990).

hanging wall is composed of mica schist and mudstone, which appear flat and less deformed away from the fault zone but become steeper and intensely deformed approaching the fault zone (Fig. 7A). This section indicates an east-west shortening direction and is characteristic of the tectonic deformation of the region.

Carboniferous and Permian strata are mainly composed of quartz sandstone, mica schist, and slate (Fig. 2). They show many lithological and structural similarities. Penetrative foliations are observed in schist and slate at Locations 6 and 7 (Figs. 2B, 7F, and 7G). Deformation fabrics such as asymmetric porphyroclasts and boudin generally indicate top-to-the-east thrusting. In addition, in the Permian strata near Xiaoheliang (Fig. 3, at Location 7), we observed basic to metabasic rocks where the internal part of the rock mass is weakly deformed. In contrast, the outer edge and small dikes are strongly deformed, showing penetrative foliation with

asymmetric porphyroclasts, similar to the adjacent deformed Permian strata.

The Early Triassic strata are generally absent. The Middle Triassic strata are dominated by neritic carbonatite deposits, with exposed dolomitic, limestone, and mudstone in unconformable contact with the underlying Permian strata. In contrast, the Late Triassic strata are dominated by intermediate-acidic volcanic formations and are in unconformable contact with the underlying strata, which is mainly magmatic and characterized by relatively weak deformation.

4. GEOCHRONOLOGY

4.1. Analytical Methods

The zircon grains analyzed were separated using standard density and magnetic separation techniques. Internal textures of these grains were examined by cathodoluminescence imag-

ing using a scanning electron microprobe at Sun Yat-sen University (SYSU, Zhuhai, China). In situ zircon U-Tu-Pb determination was carried out using an iCAP-RQ inductively coupled plasma-mass spectrometer (ICP-MS) coupled with an ArF-193 nm GeolasHD laser ablation (LA) system at the SYSU. A spot size of 32 μm with a laser repetition rate of 5 Hz was used to ablate the zircons. Off-line raw data were processed using the GLITTER program (Van Achterbergh et al., 1999; Griffine et al., 2008), and isotopic apparent and weighted mean ages were calculated using the Isoplot program (Ludwig, 2003). Zircon ages with a calculated discordance of <10% are considered to be valid, and $^{207}\text{Pb}/^{206}\text{Pb}$ and $^{206}\text{Pb}/^{238}\text{U}$ apparent ages of the older (>1 Ga) and younger (<1 Ga) zircon grains are presented, respectively.

The mica sample used for $^{40}\text{Ar}/^{39}\text{Ar}$ analyses was individually wrapped in Al-foil packets, encapsulated in sealed Gd foil, and irradiated in

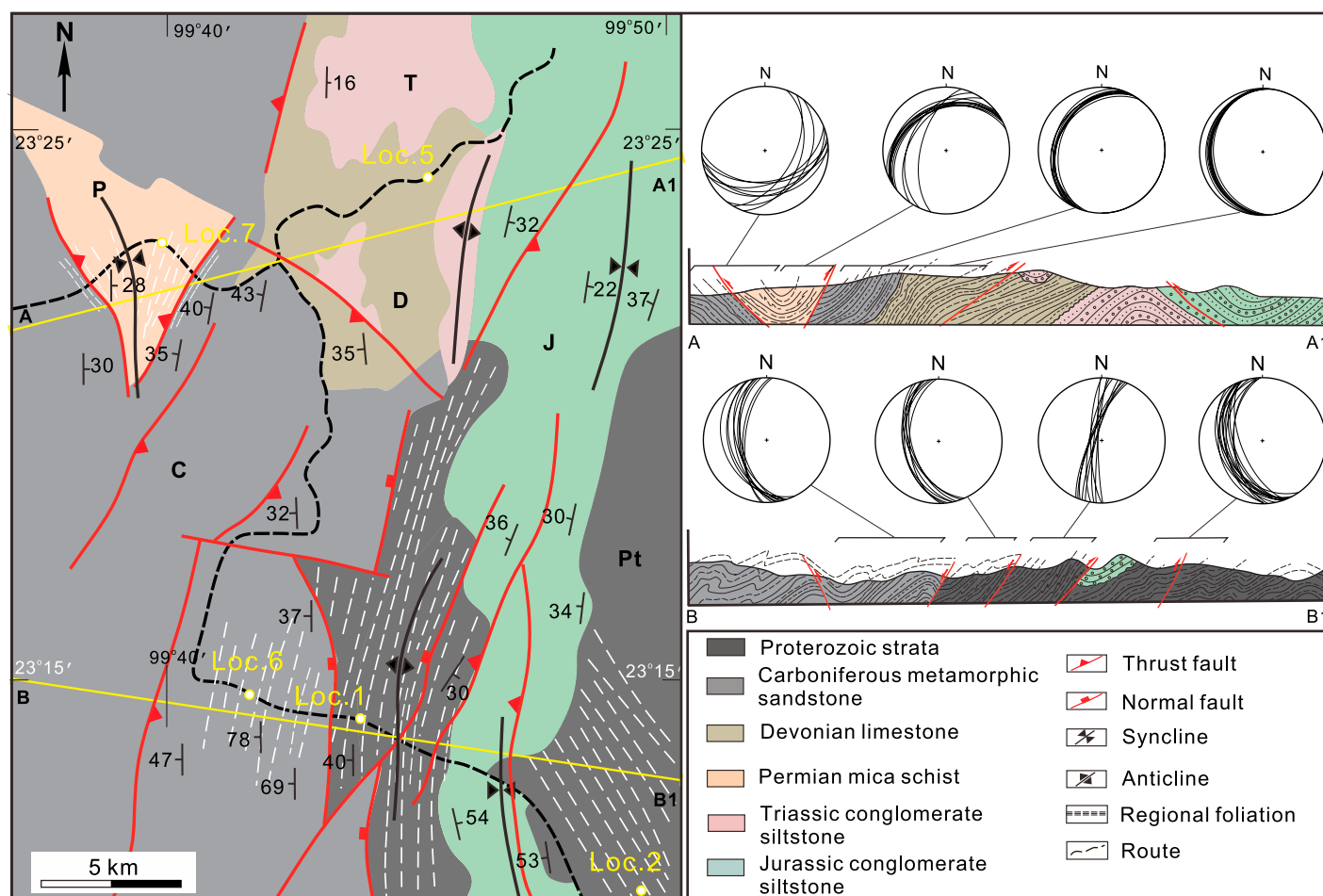


Figure 3. Detailed field mapping and geological cross sections of the Xiaoheijiang region (BGMRYP, 1990). C—Carboniferous; D—Devonian; J—Jurassic; Loc.—Location; P—Permian; Pt—Proterozoic; T—Triassic.

the central thimble position of the nuclear reactor (1000 kW) for 2627 min with an instantaneous neutron flux of $6.63 \times 10^{12} \text{ n}/(\text{cm}^{-2} \text{ s}^{-1})$ at the Chinese Academy of Atomic Energy Science. After irradiation, the sample was degassed and purified in steps. The $^{40}\text{Ar}/^{39}\text{Ar}$ measurement was carried out on a GV Instruments 5400 MS at the Guangzhou Institute of Geochemistry, Chinese Academy of Sciences. The detailed analytical techniques for these MS analyses are described by Qiu and Wijbrans (2008). The $^{40}\text{Ar}/^{39}\text{Ar}$ dating results were calculated and plotted using the Ar-ArCALC software (Koppers, 2002). Plateau ages were determined from three or more contiguous steps, comprising $>50\%$ of the ^{39}Ar released and revealed concordant ages at the 95% confidence level (McDougall and Harrison, 1999).

4.2. U-Pb Geochronology

Sample 21YN-6, collected from a metagabbro (at Location 7; Figs. 3 and 7B; $23^\circ 22.834'\text{N}$,

$99^\circ 39.568'\text{E}$), exhibits foliations and ductile shearing fabrics that are consistent with the surrounding Permian mica schist. The main minerals observed are pyroxene (35%–40%), amphibole (25%–30%), feldspar (15%–20%), mica, and minor quartz. Preferred biotite orientation and asymmetric porphyroclasts are observed at the microscopic scale (Figs. 7C and 7D). Most zircon grains separated from this sample have lengths of 100–200 μm with length/width ratios of ~ 1 –1.5 (Fig. 7H). Computed laminographic (CL) images show two groups: the magmatic zircons are colorless and transparent and show apparent oscillatory zoning, and the metamorphic zircons are gray-black with poor zonation (Fig. 7H; Hoskin and Schaltegger, 2003). Twenty-four analyses were conducted in this sample, and four grain data points with a disagreement of $>20\%$ were excluded from the mean calculation (Table 1). Eleven spot analyses lie on or below the Concordia line, with $^{206}\text{Pb}/^{238}\text{U}$ ages ranging from 1846 Ma to 411 Ma, which correspond to

those of the inherited zircons. The remaining eight concordant data yield a weighted mean $^{206}\text{Pb}/^{238}\text{U}$ age of 230 ± 3.1 Ma with a mean square of weighted deviates (MSWD) of 0.17 (Fig. 7H), which is interpreted to represent the deformation and metamorphic timing of the metagabbro.

4.3. $^{40}\text{Ar}/^{39}\text{Ar}$ Dating

To constrain the timing of metamorphism and deformation identified along the Lancang metamorphic complex, three samples collected from mica schists and mylonites with E-W-directed shortening deformation fabrics were analyzed for $^{40}\text{Ar}/^{39}\text{Ar}$ geochronology.

Sample 09YN-43 is a Proterozoic mica schist, which exhibits pervasive foliations that dip toward the west (at Location 2; Fig. 4; $23^\circ 14.410'\text{N}$, $99^\circ 41.595'\text{E}$). The quartz grains were sheared asymmetrically (Fig. 4E). Some feldspars have undergone intense ductile shearing that formed asymmetric porphyroclasts

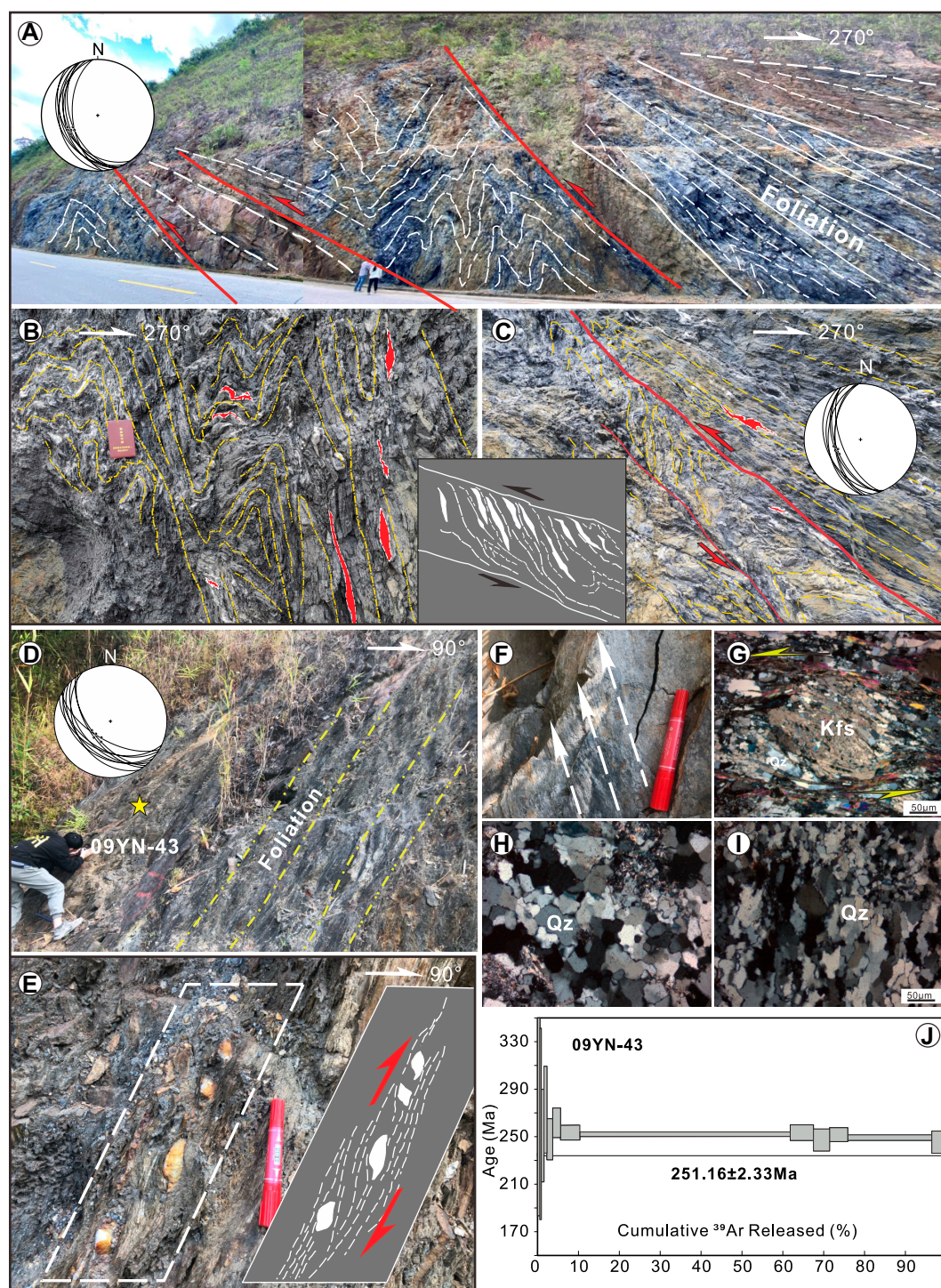


Figure 4. (A) Field photographs of typical crustal shortening fabrics in the Proterozoic strata along the Lancang metamorphic complex. (B, C) Asymmetric folds, penetrative foliation, and S-C fabrics in Proterozoic strata. (D, F) Penetrative foliations and lineations at sites of sample 09YN-43. (E) Typical asymmetric quartz porphyroclasts associated with crustal shortening. (G) Microstructures of sample 09YN-43 show intense ductile shearing of the feldspars (Kfs) and formation of asymmetric porphyroclasts. (H, I) The quartz (Qz) grains show sweeping undulose extinction and strongly elongated bands that are indicative of grain boundary migration recrystallization. (J) Age spectra for muscovite from sample 09YN-43; plateau age is reported within 2σ error.

(Fig. 4G). The quartz grains are marked by sweeping undulose extinction and have irregular grain shapes and grain sizes, which are indicative of grain boundary migration (GBM) recrystallization (Figs. 4H and 4I). The release spectrum for muscovite grains from sample 09YN-43 yields a flat plateau age of 251.16 ± 2.33 Ma that accounts for 95% of the released ^{39}Ar (steps 5–13; Fig. 4J).

Sample 09YN-13 was collected from the Paleozoic mylonite located to the southwest of Yunxian County (at Location 3; Fig. 2A; $24^{\circ}22.752'\text{N}$, $100^{\circ}03.427'\text{E}$). It exhibits a quartz-biotite-feldspar assemblage and preserves asymmetric porphyroclasts (Fig. 5B). Quartz grains vary from $10\text{ }\mu\text{m}$ to $500\text{ }\mu\text{m}$ in size and show apparent undulatory extinction and elongation (Figs. 5B and 5C). Finer

grains were formed from the host grain by bulging recrystallization along the grain boundaries (Fig. 5C). The feldspars in the mylonite exhibit brittle fractures that display domino-type fragmented porphyroclasts (Fig. 5E). Sericite grains from this sample yield a plateau age of 234.31 ± 2.97 Ma, which amounts to $\sim 85\%$ of the ^{39}Ar released (steps 7–21; Fig. 5D).

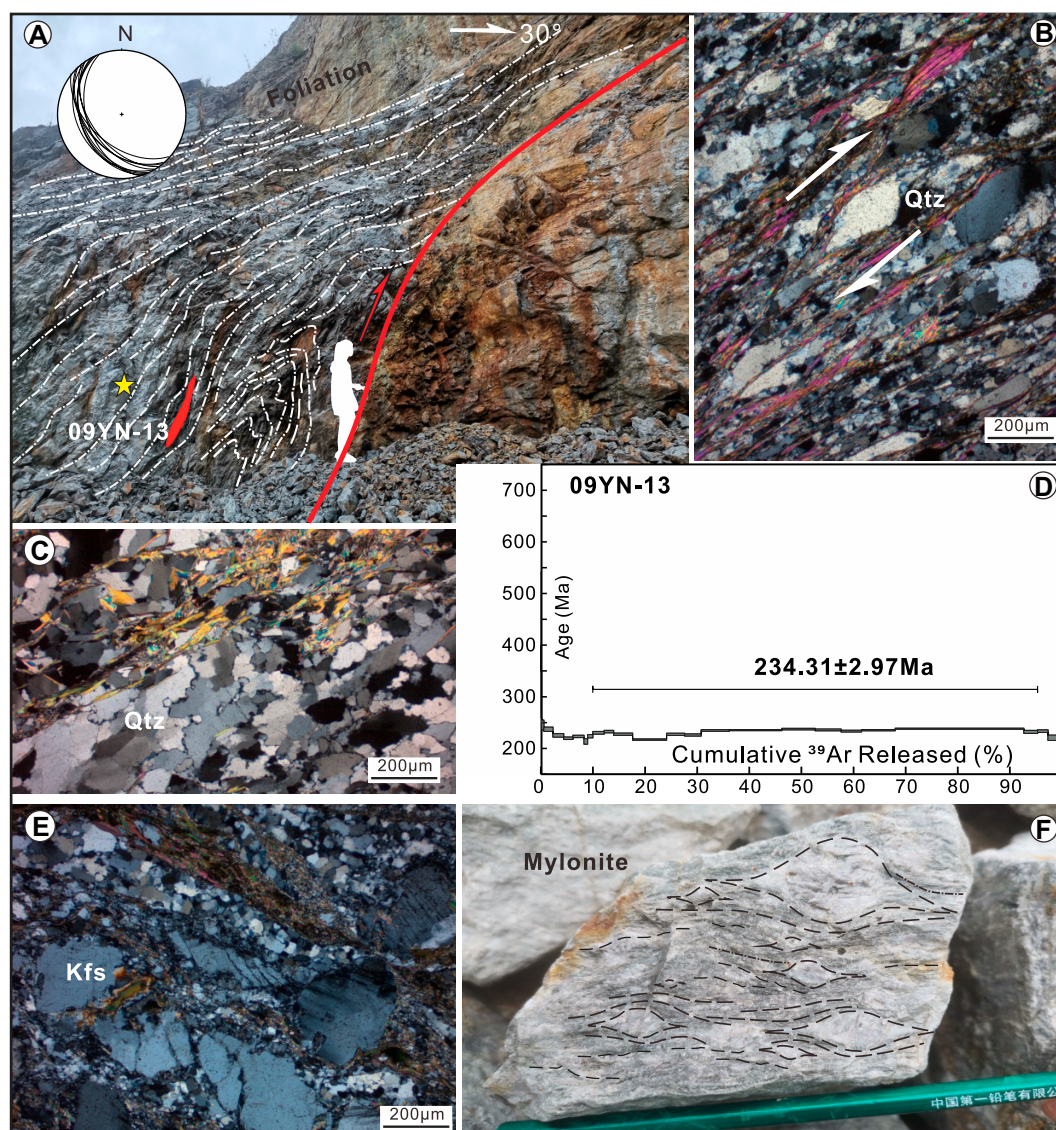


Figure 5. (A) Photograph showing Paleozoic mylonites with penetrative foliations and asymmetric folds. (B, C, E) Microstructures in quartz (Qtz) from sample 09YN-13, showing asymmetric porphyroclasts, undulate extinction, bulging, and feldspars (Kfs) that are brittle and fractured with domino-type fragments. (D) $^{40}\text{Ar}/^{39}\text{Ar}$ plateau age of sample 09YN-13. (F) Asymmetric quartz porphyroclasts in the mylonite.

Sample 09YN-20 was taken from an Ordovician sericite schist that exhibits pervasive foliations dipping toward the northeast (Location 4; Fig. 2A; $24^{\circ}38.532'\text{N}$, $99^{\circ}46.745'\text{E}$). The quartz and feldspar veins have undergone intense ductile shearing, forming asymmetric boudins and S-C fabrics. The mineral assemblage of samples analyzed includes quartz, feldspar, sericite, biotite, and minor muscovite. Quartz grains show undulatory extinction (Fig. 6F and 6G). Some large quartz grains are observed to be surrounded by fine subgrains or newly recrystallized fine grains that form a core-mantle structure (Figs. 6F and 6G). The release spectrum for sericite grains from sample 09YN-20 exhibits an approximately flat portion (steps 5–11, including $\sim 60\%$ of the ^{39}Ar released) with a corresponding plateau age of 234.92 ± 4.10 Ma (excluding the first four low-temperature steps; Fig. 6E).

5. DISCUSSION

5.1. Timing Constraints on Deformation and Metamorphism of the Lancang Metamorphic Complex

The Lancang metamorphic complex was likely located in the fore-arc region during the subduction of the Paleo-Tethys Ocean, since the Lancang granite belt to the east is generally interpreted as the island arc of the subduction system (e.g., Wang et al., 2010, 2018b; Peng et al., 2013; Deng et al., 2018; Zhai et al., 2019). In addition, the metabasites in the Damanguangfang and Xiaohaijiang counties along the Lancang metamorphic complex yield zircon U-Pb ages of 270–264 Ma and display both MORB- and arc-like signatures that are suggestive of a Permian fore-arc setting related to subduction of the Paleo-Tethys Ocean (e.g., Jian et al., 2009a,

2009b; Wang et al., 2018b). Our new structural observations reveal that the intense crustal shortening and greenschist- to amphibolite-facies metamorphism may have occurred along the Lancang metamorphic complex, which formed regional foliations and shortening structures such as folds and thrusts at various scales. In addition, $^{40}\text{Ar}/^{39}\text{Ar}$ and zircon U-Pb data obtained in this study put timing constraints on the deformation episodes related to the subduction and subsequent collision of the Paleo-Tethys Ocean.

Sample 21YN-6 is a highly deformed metagabbro, and its penetrative foliations, lineations, and asymmetric porphyroclasts all point to a nearly E-W-directed compression (Figs. 7B and 7E). The inheritance zircons yield an age of 1846–411 Ma. However, the gray-black metamorphic zircons with poor zonation yield a weighted mean $^{206}\text{Pb}/^{238}\text{U}$ age of 230 ± 3.1 Ma (MSWD = 0.17; Fig. 7H). By combining field-

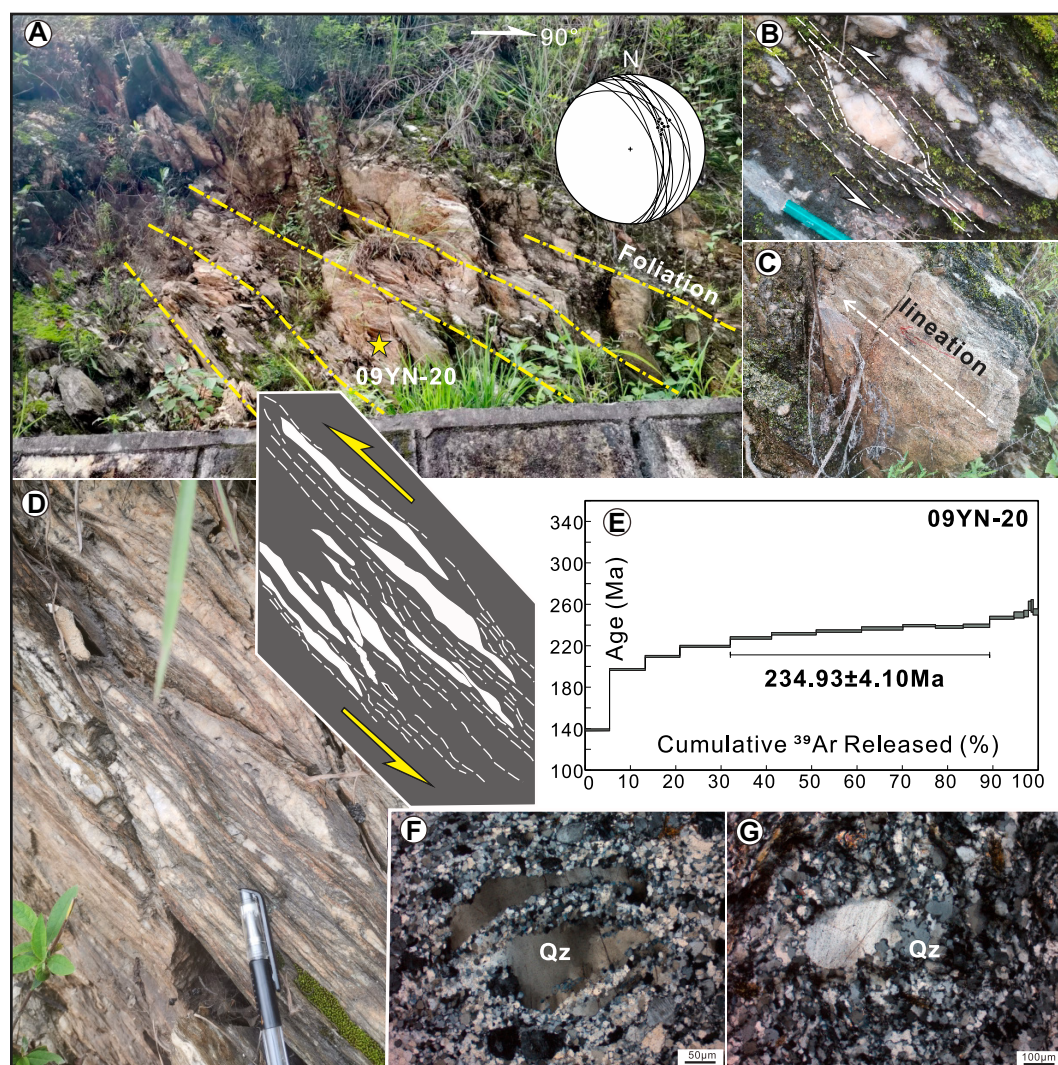


Figure 6. (A) Photograph of Ordovician strata with penetrative foliations. (B, C, D) Asymmetric boudins and lineations indicating E-W-directed thrusting. (E) $^{40}\text{Ar}/^{39}\text{Ar}$ plateau age of mica in 09YN-20. (F, G) Microstructure in the sample analyzed displaying undulate extinction, bulging, and core-mantle structures of quartz (Qz) grains.

and microscopic-scale observations, the age of this sample is interpreted to represent the timing of E-W-directed shortening during the subduction-collision stage of the Paleo-Tethys Ocean.

Sample 09YN-43, which was collected from the Proterozoic mica schist, yields a $^{40}\text{Ar}/^{39}\text{Ar}$ plateau age of $251.16 \pm 2.33 \text{ Ma}$ (Fig. 4J). Penetrative foliations, asymmetric folds, boudins, and porphyroclasts all indicate an E-W-directed crustal shortening (Figs. 4D and 4E). At the microscopic scale, quartz crystals exhibit wave extinction and polycrystalline quartz grains with irregular grain boundaries that developed in response to GBM recrystallization (Figs. 4H and 4I), and the feldspars underwent ductile shearing to form porphyroclasts (Fig. 4G). These microfabrics are likely indicative of a deformation temperature of 400–500 °C (Stipp et al., 2002), which is higher than the closure temperature of sericite in the $^{40}\text{Ar}/^{39}\text{Ar}$ system (~350 °C; Harrison et al., 1985). Therefore, the plateau age of $251.16 \pm 2.33 \text{ Ma}$ could be interpreted

as a cooling age that approximates or is slightly younger than the timing of the crustal shortening stage, which likely occurred during subduction or collision.

Sample 09YN-13 was taken from a Paleozoic mylonite and yields a $^{40}\text{Ar}/^{39}\text{Ar}$ plateau age of $234.3 \pm 3.0 \text{ Ma}$. Sample 09YN-20, collected from an Ordovician mica schist, exhibits a $^{40}\text{Ar}/^{39}\text{Ar}$ plateau age of $234.9 \pm 4.1 \text{ Ma}$. At the outcrop scale, folded gneissic and mica schist foliations are observed near the sample sites. Together with asymmetric boudins and S-C fabrics, these observations also indicate E-W-directed shortening. Asymmetric quartz and feldspar porphyroclasts and mica fish exhibit consistent kinematics (Figs. 5B and 5F). In addition, quartz grains in the sample analyzed show strong shape-preferred orientation, undulatory extinction, and bulging and core-and-mantle structures (Figs. 5C, 6F, and 6G). Feldspars exhibit brittle fractures and display domino-type fragmented porphyroclasts (Fig. 5E). These microfabrics

from the two samples indicate a deformation temperature of 300–400 °C (Stipp et al., 2002). The biotite $^{40}\text{Ar}/^{39}\text{Ar}$ system would likely have been fully reset during this phase of deformation (McDougall and Harrison, 1999). Thus, the plateau ages of 09YN-13 and 09YN-20 likely represent the timing of crustal shortening.

5.2. Evolution of the Paleo-Tethys Ocean in the SE Tibetan Plateau

Our new data from petrology, structural analysis, and geochronology, combined with data from previous studies, enable us to retrace the deformation history of the Lancang metamorphic complex as well as the evolution of the Paleo-Tethys Ocean. Existing chronologic data suggest that the opening of the Paleo-Tethys Ocean may have begun during the Middle Devonian, as recorded by the earliest pelagic sediments and ophiolite complex (e.g., Feng and Liu, 1993; Duan et al., 2006; Metcalfe, 2013). Continued

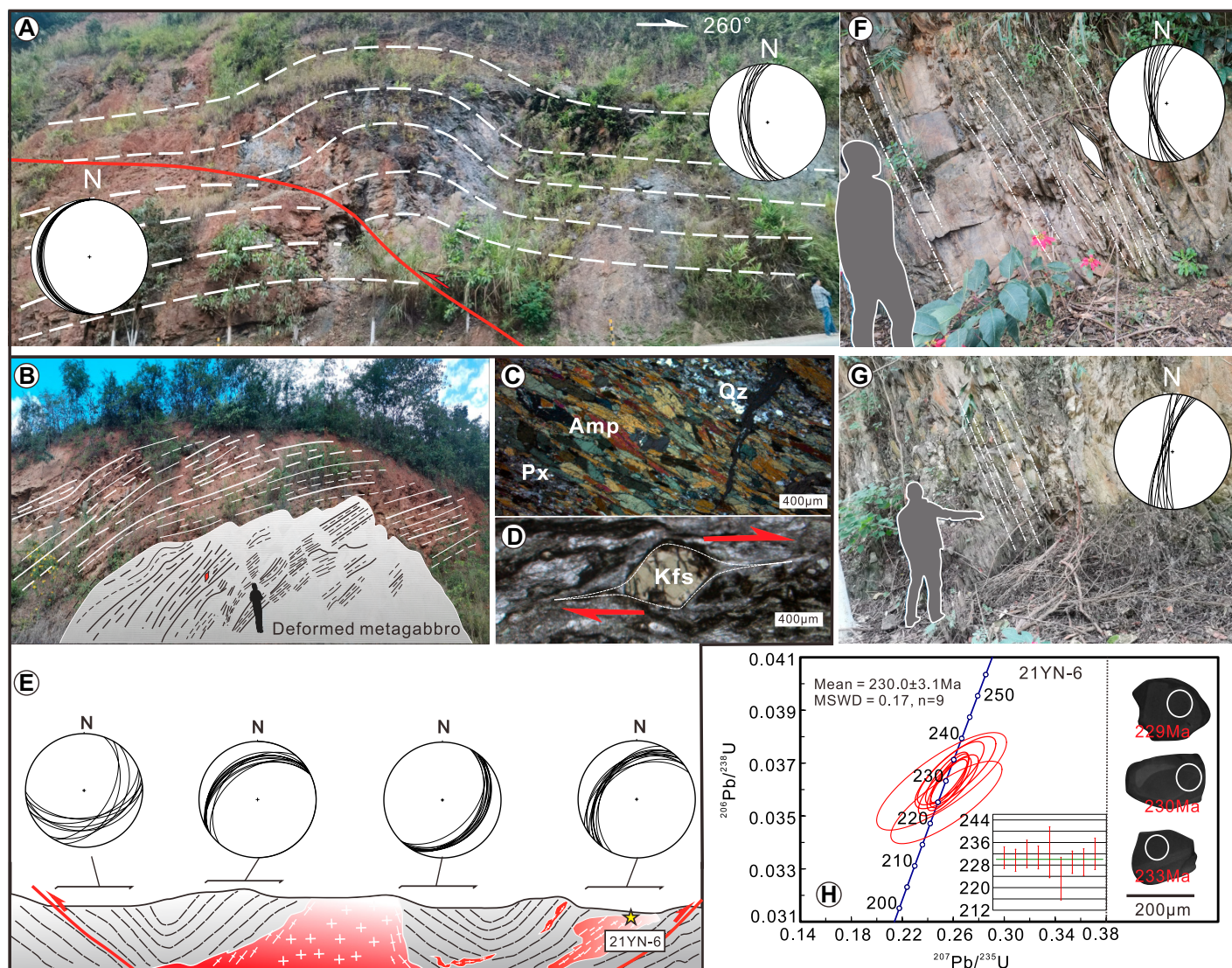


Figure 7. (A) Dashed white lines indicate the flat-ramp structure that developed in the Devonian strata. (B, F) Field deformation fabrics with penetrative foliation in the Permian strata. (C, D) Microstructure of sample 21YN-6 showing intense mineral stretching and asymmetric feldspar porphyroclasts. (E) Geological cross section of the sample site. (G) Photograph of penetrative foliation, cleavages, and asymmetric boudin in the Carboniferous strata. (H) Zircon U-Pb age of sample 21YN-6 and zircon cathodoluminescence photos. Amp—amphibolite; Px—pyroxene; Qz—quartz; Kfs—K-feldspar; MSWD—mean square of weighted deviates.

subduction of the Paleo-Tethys Ocean likely altered the overlying mantle wedge, resulting in melting and the formation of a magma arc in the western margin of the Simao block and the opening of an oceanic back-arc basin (e.g., Peng et al., 2008; Hennig et al., 2009; Deng et al., 2014, 2018; Wang et al., 2019). However, the timing of the onset of the subduction still remains controversial. Metcalfe (2006, 2011, 2013) and Sone et al. (2012) proposed that the initial subduction beneath the Indochina block likely started during the latest Carboniferous–Early Permian and continued until the Middle Triassic. On the other hand, Deng et al. (2018) proposed that the subduction initiated during

the Late Carboniferous and continued until the Permian–Early Triassic.

In western Yunnan, the evidence for subduction includes the following. (1) Pelagic radiolarian cherts within the Changning–Menglian suture zone (representing the main Paleo-Tethys Ocean basin) that range in age from late Middle Devonian to Middle Triassic (Fig. 8A; e.g., Metcalfe, 2013, 2021; Wang et al., 2018b). (2) The magmatic arc rock units in the Jinghong and Yunxian regions are enriched in large ion lithophile elements and light rare earth elements and depleted in high field strength elements, similar to the typical subduction-related arc volcanic rocks, which were dated at 284–249 Ma

by zircon LA-ICP-MS analyses (e.g., Mo et al., 1998; Peng et al., 2008; Hennig et al., 2009). (3) The Nanlinshan volcano-plutonic rocks display MORB-like geochemical affinity and yield a U-Pb zircon age of 298–290 Ma (e.g., Hennig et al., 2009; Li et al., 2012; Keller et al., 2015; Wang et al., 2015), and meanwhile, the associated granodiorites at adjacent sites are dated at 284–282 Ma (Hennig et al., 2009). (4) The Banpo–Yakou–Jinghong mafic-ultramafic complexes (south of the Lincang granite belt), which were interpreted to form in a back-arc setting, yield zircon U-Pb ages of 315–264 Ma (e.g., Wang et al., 2015; Jian et al., 2009a, 2009b; Li et al., 2012; Zhai et al., 2019). (5) The metabas-

TABLE 1. LASER ABLATION–INDUCTIVELY COUPLED PLASMA–MASS SPECTROMETRIC ZIRCON U–PB DATA FROM THE XIAOHEIJIANG METAGABBROS IN THE LANCANG METAMORPHIC COMPLEX

Th/U analysis spot	Isotopic ratios						Apparent age (Ma)						Concordance
	²⁰⁷ Pb/ ²⁰⁶ Pb		²⁰⁷ Pb/ ²³⁵ U		²⁰⁶ Pb/ ²³⁸ U		²⁰⁷ Pb/ ²⁰⁶ Pb		²⁰⁷ Pb/ ²³⁵ U		²⁰⁶ Pb/ ²³⁸ U		
	1σ		1σ		1σ		1σ		1σ		1σ		
21YN-6 metagabbros, mean age = 230 ± 3.1 Ma													
21YN-6-01	0.53	0.10734	0.0028	3.96876	0.1084	0.26851	0.00428	1755	47	1628	22	94%	
21YN-6-02	2.85	0.06392	0.00219	1.05378	0.03679	0.11972	0.00202	739	71	731	18	100%	
21YN-6-03	0.46	0.05606	0.00201	0.53755	0.0196	0.06965	0.00118	454	78	437	13	99%	
21YN-6-04	0.38	0.05133	0.00194	0.25735	0.00987	0.03641	0.00062	256	85	233	8	99%	
21YN-6-05	0.25	0.05166	0.00212	0.25797	0.01066	0.03627	0.00063	271	91	233	9	99%	
21YN-6-06	2.36	0.10925	0.00338	3.75936	0.12042	0.24996	0.00423	1787	55	1584	26	91%	
21YN-6-07	0.25	0.0599	0.00222	0.54391	0.02051	0.06596	0.00114	600	78	441	13	93%	
21YN-6-08	0.19	0.05118	0.00346	0.25804	0.01727	0.03662	0.00079	249	149	233	14	99%	
21YN-6-09	0.97	0.05086	0.00221	0.25509	0.01115	0.03643	0.00065	235	97	231	9	100%	
21YN-6-10	0.58	0.06351	0.00246	0.62333	0.02447	0.07129	0.00126	726	80	492	15	90%	
21YN-6-11	0.66	0.05068	0.0081	0.25622	0.0401	0.03673	0.00145	226	333	232	32	100%	
21YN-6-12	0.77	0.05408	0.00714	0.26231	0.03388	0.03524	0.00121	374	273	237	27	94%	
21YN-6-13	0.62	0.05128	0.00206	0.25528	0.01041	0.03617	0.00064	253	90	231	8	99%	
21YN-6-14	0.99	0.10738	0.00378	4.71697	0.17128	0.31917	0.00562	1755	63	1770	30	101%	
21YN-6-15	0.79	0.05655	0.0024	0.51239	0.02206	0.06584	0.00122	473	92	420	15	98%	
21YN-6-16	0.61	0.11493	0.00417	5.11861	0.19151	0.32358	0.00575	1879	64	1839	32	98%	
21YN-6-17	0.56	0.10729	0.004	4.17472	0.16029	0.28271	0.0051	1754	67	1669	31	96%	
21YN-6-18	0.49	0.05148	0.00313	0.25623	0.01555	0.03616	0.00076	263	134	232	13	99%	
21YN-6-19	0.22	0.13902	0.00525	6.34241	0.24661	0.33148	0.00603	2215	64	2024	34	91%	
21YN-6-20	0.81	0.05191	0.0042	0.26174	0.02093	0.03664	0.0009	281	175	236	17	98%	

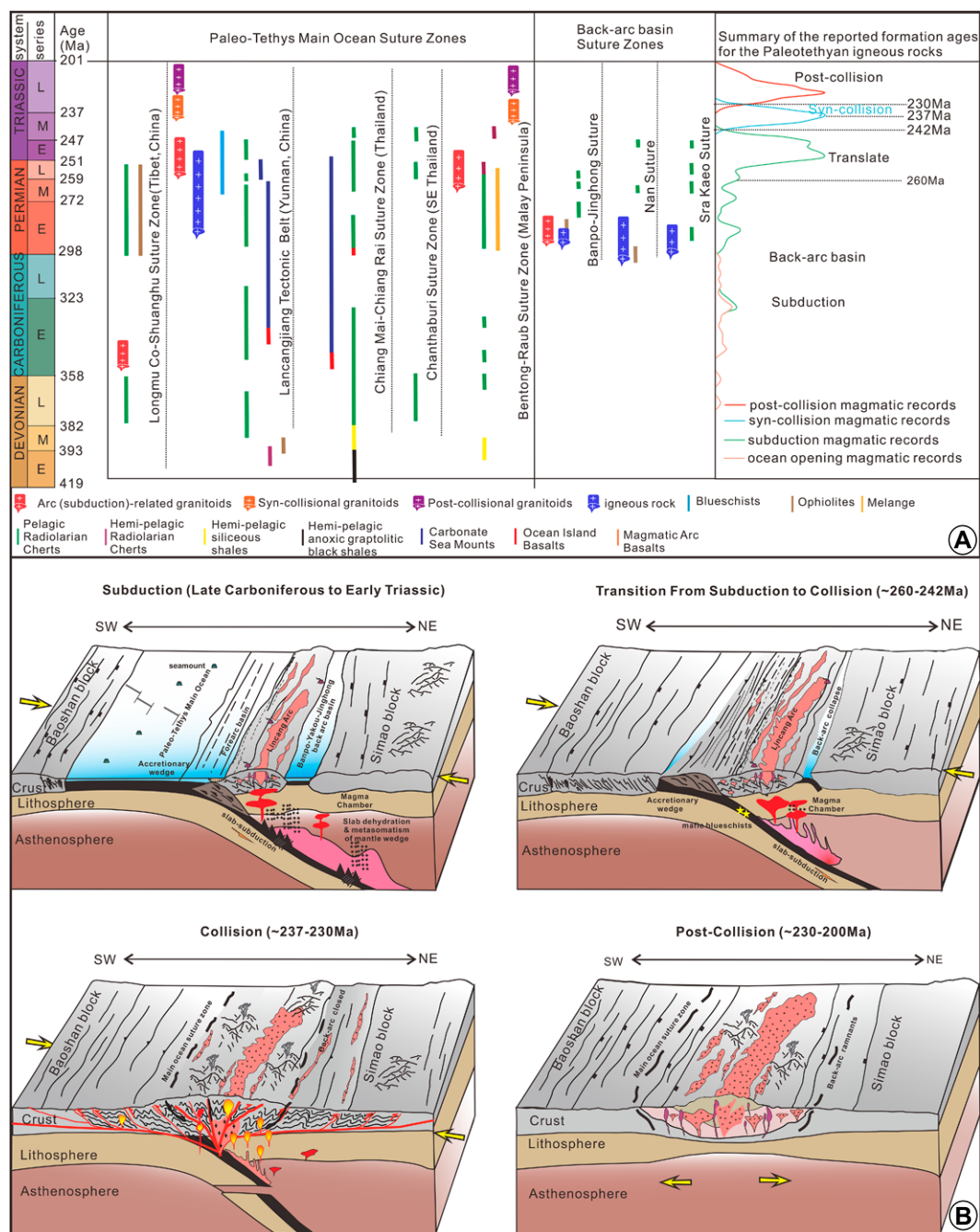
sic rocks in the Niujiangshan ophiolite give zircon U–Pb ages of 272–264 Ma and have both volcanic arc basalt and MORB geochemical characteristics and were considered to be supra-subduction zone-type ophiolite that corresponds to the subduction of the oceanic crust (Jian et al., 2009a). Similar evidence also exists in Southeast Asia. In Thailand, Laos, and Cambodia on the Indochina Peninsula, the basaltic rocks and ophiolites related to the back-arc basin give an age of 320–260 Ma and could possibly be connected to the Banpo–Jinghong areas (e.g., Hara et al., 2020; Ueno and Hisada, 2001; Wang et al., 2020b). Additionally, arc-related igneous rocks yield U–Pb ages of 296–238 Ma, and the granitoids were dated at 289–244 Ma (e.g., Hara et al., 2020; Metcalfe, 2013; Qian et al., 2016a, 2016b; Wang et al., 2020c). Based on the evidence above, the subduction of the Paleo-Tethys Ocean likely occurred in the Late Carboniferous–Early Triassic (Figs. 8A and 8B).

Since ca. 260 Ma, seamount-like material may have been subducted to a depth of 30–35 km (at conditions of ~450 °C, ~0.9 GPa) and experienced high-pressure, low-temperature blueschist-facies metamorphism at ca. 248–242 Ma (e.g., Fan et al., 2015; Wan et al., 2019; Wang et al., 2019). Subsequently, this material may have exhumed to the shallow crust due to the juxtaposition of nappe structures during the Middle Triassic (e.g., Fan et al., 2015; Wang et al., 2018a). The rapid exhumation of the blueschists may represent the onset of collision (Fan et al., 2015). The Jinghong–Manbing arc granodiorite and amphibolite in the southern segment of the Lincang granite belt yield zircon U–Pb ages of 259–242 Ma and show characteristics of calc-alkaline I-type granitoids and typical island arc magmatic rocks, which were interpreted to have formed during the transition from slab

subduction to collision (e.g., Wang et al., 2015; Sun et al., 2020). The Chiang Khong volcanic rocks in northwestern Thailand, which are characterized by arc volcanic rocks and interpreted to be the product of the tectonic transition from arc to collisional stages, yield U–Pb ages of 242–238 Ma (Qian et al., 2013). In addition, the fore-arc region may have experienced crustal compression and metamorphism, forming penetrative regional foliations and shortening structures during the transition stage. Our new ⁴⁰Ar/³⁹Ar data from the Proterozoic mica schist yield a plateau age of 251.16 ± 2.33 Ma, which likely represents the timing of E–W–directed shortening. Wang et al. (2022) reported a deformation age of 248 Ma at nearby sites that is consistent with our data. Therefore, combined with the age cluster of the metamorphic rocks in the Lancang metamorphic complex (260–240 Ma; e.g., Fan et al., 2015; Bi et al., 2018; Wang et al., 2020a, 2020b, 2021), we argue that the Paleo-Tethys Ocean experienced a transition stage from slab subduction to continental collision from ca. 260 Ma to 242 Ma in the SE Tibetan Plateau (Fig. 8B; e.g., Peng et al., 2013; Jian et al., 2009a, 2009b; Wang et al., 2010; Deng et al., 2018). Another key issue is whether the Banpo–Jinghong back-arc basin closed during this stage. The Banpo–Jinghong back-arc basin includes deep-marine radiolarian cherts of Early to Late Permian age (Fig. 8A; e.g., Feng and Liu, 1993; Li et al., 2012; Zhai et al., 2019), but there are no records from the Triassic or later. Therefore, we speculate that the back-arc basin may have collapsed during this stage.

The next stage is the closure of the Paleo-Tethys Ocean and subsequent continental collision. However, the collision processes and timing are controversial. Wang et al. (2018b) proposed that the Baoshan–Sibumasu block

began to collide with the Simao–Indochina block in the Middle Triassic period (ca. 237 Ma) based on magmatic and metamorphic records in western Yunnan and Southeast Asia and resulted in the final closure of the Jinghong–Nan–Sa Kao back-arc basins. The major collision phase of the Paleo-Tethys Ocean occurred during the Middle–Late Triassic period (ca. 237–230 Ma) and resulted in the formation of a united proto–Southeast Asia continent (Wang et al., 2018b). Metcalfe (2013, 2021) synthesized the stratigraphy, paleontology, and structure of the Paleo-Tethys domain, suggesting that the back-arc basin began to collapse due to the subduction-collision of the Paleo-Tethys Ocean in the Late Permian to Middle Triassic (256–240 Ma). Collision of the Sibumasu block, Sukhothai, and Indochina may have occurred in the Middle Triassic to Late Triassic, leading to the final closure of the Sukhothai back-arc basin in the Late Triassic and the formation of widespread S-type granites in Thailand on the Malay Peninsula. However, deep-water sediments between Sibumasu and the Sukhothai block up to at least ca. 236 Ma were identified in Thailand, and Late Triassic turbidite deposition was also observed on the Sukhothai arc (Morley, 2018), which suggests that the collision may have occurred in the Late Triassic or after. In addition, there is magmatism that is related to the Early–Middle Triassic collision in Thailand. Therefore, Morley (2018) proposed that the early collision during the Early–Middle Triassic occurred between the Sibumasu block and the Sukhothai arc. In the latest Triassic or even Early Jurassic, the back-arc basin closed, leading to the final assemblage between the Sibumasu, Sukhothai arc, and Simao–Indochina. We cannot determine which model is most accurate, and these models are not mutually exclusive. The eastern Paleo-



Tethys Ocean extends >1000 km in the SE Tibetan Plateau and SE Asia, and the collision processes and timing may vary spatially. We argue that the collision stage in western Yunnan may have occurred during 237–230 Ma based on the following magmatic, structural, and chronologic observations. First, the high-K calc-alkaline S-type granites in the Lincang granite belt with a main age peak of 237 Ma were generally interpreted as syn-collisional products (e.g., Jian et al., 2003, 2009a; Wang et al., 2014b; Fan et al., 2015; Qian et al., 2016b; Wang et al.,

2016b, 2018b). In addition, Manghuai volcanic rocks (mainly composed of rhyolites) have geochemical characteristics similar to those of Lincang granites and yield a zircon U-Pb age of 241–231 Ma that was also likely generated from the syn-collisional stage (e.g., Peng et al., 2008, 2013; Fan et al., 2009; Wang et al., 2012). Second, the sedimentary rocks within the Lincang metamorphic complex and adjacent regions generally experienced variable deformation and metamorphism during this period. The metamorphic zircon from polysilicon musco-

vite schist yields U-Pb ages of 238–231 Ma that indicate the timing of the peak metamorphism (e.g., Li et al., 2017; Wang et al., 2020a). Third, our structural and geochronologic data reveal intense crustal deformation along the Lincang metamorphic complex that led to the formation of regional foliations, thrusts, macroscale and mesoscale folds of foliated rocks, and other ductile-brittle fabrics. Metagabbro, schist, and mylonite, which preserve deformation fabrics indicating E-W-directed shortening, yield U-Pb and $^{40}\text{Ar}/^{39}\text{Ar}$ ages of 234–230 Ma. However, it

remains uncertain whether continental collision or continent-arc collision occurred in the SE Tibetan Plateau. Middle and Late Triassic deep-sea sediments were not found along the Lancangjiang belt and adjacent regions; the records of the Banpo-Jinghong back-arc pelagic radiolarian cherts only continued to the Late Permian (Fig. 8A). Therefore, we speculate that the back arc may have closed in the Early Triassic, and the major stage of collision between Baoshan and Simao most likely occurred around 237–230 Ma (Fig. 8B).

Following the collision, the Paleo-Tethys domain entered the post-collision extensional phase in the Late Triassic (e.g., Morley, 2018; Wang et al., 2018b). The crustal shortening may have switched to regional extension, accompanied by upwelling of the asthenospheric mantle, which resulted in the partial melting of crustal material and formed the Lincang granite belt to the east of the Lancang metamorphic complex. The Late Triassic granitoids range from 230 Ma to 203 Ma and have geochemical characteristics that mainly plot in the post-collisional fields and exhibit high-K calc-alkaline and A-type granite signatures (Deng et al., 2018). For example, the Mengsong (228–222 Ma) and Bulangshan (218–216 Ma) granites from the southern extension of the Lincang Batholith were all interpreted to be generated in a post-collision extensional setting (e.g., Wang et al., 2015; Deng et al., 2018). Granites in northwestern Laos that yield zircon ages of 231–220 Ma belong to the high-K calc-alkaline A-type series and were derived from a mixed source and formed in a post-collisional setting (Qian et al., 2016a; Wang et al., 2018b). Volcanic rocks of the Xiaodingxi formation (220–214 Ma) and Manghuihe formation (216–210 Ma) are mainly of the high-K calc-alkaline basalt series, which is characteristic of post-collision magmatic assemblages (e.g., Kong et al., 2012; Nie et al., 2016; Dong et al., 2013; Peng et al., 2013; Wang et al., 2014a; Fan et al., 2009). In addition, the post-collision volcanic rocks are also exposed in the Chiang Khong–Lampang–De igneous rock belt in NW Thailand and yield zircon U–Pb ages of 229–220 Ma (Qian et al., 2016b; Wang et al., 2018b). Metamorphic zircon U–Pb ages and polysilicon muscovite $^{40}\text{Ar}/^{39}\text{Ar}$ data constrain the retrograde age of widely exposed metasedimentary rocks to 222–207 Ma (Wang et al., 2020a, 2021). These high-pressure–ultrahigh-pressure rocks may have experienced a rapid exhumation to the shallow crust due to post-orogenic extension during this period. Therefore, all of the evidence indicates that the Paleo-Tethys domain may have entered the post-collision stage during 230–200 Ma (Fig. 8B).

6. CONCLUSIONS

The Lancang metamorphic complex, together with the Changning–Menglian suture, Lincang igneous belt, and Banpo–Jinghong back-arc system, constitutes the Lancangjiang tectonic belt, which records the tectonic evolution of the eastern Paleo-Tethys domain. Penetrative regional foliations, thrusts, asymmetric folds at various scales, and ductile shearing fabrics are observed within the Lancang metamorphic complex. Ar–Ar and U–Pb dating indicate that the intense E–W–directed contractional deformation occurred between 251 Ma and 230 Ma and probably encompasses subduction- and collision-related deformation. A synthesis of existing magmatic and metamorphic data and our new structural geochronologic observations point to four stages of evolution of the eastern Paleo-Tethys domain in the SE Tibetan Plateau. Subduction of the Paleo-Tethys Ocean may have continued from the Late Carboniferous to Early Triassic and formed the trench-arc basin system in SE Tibetan Plateau. During 260–242 Ma, the Paleo-Tethys entered the subduction-collision transitional stage, and the main collision occurred at 237–230 Ma. Crustal shortening may have switched to regional extension at 230–200 Ma, resulting in post-collision magmatic activity along the N–S–striking Lincang granite belt.

ACKNOWLEDGMENTS

We sincerely thank two reviewers for their thorough and critical reviews. We also thank editors Wenjiao Xiao and Yongjiang Liu for editorial handling and constructive comments. This research was supported by the National Natural Science Foundation of China (41830211 and 42272247), the Guangdong Basic and Applied Basic Research Foundation (2018B030312007), the Southern Marine Science and Engineering Guangdong Laboratory (Zhuhai: 311022010), Guangdong Province Introduced Innovative R&D Team of Geological Processes and Natural Disasters around the South China Sea (2016ZT06N331), the Fundamental Research Funds from the Central Universities to Sun Yat-sen University (23lgjb013, 22lgjb14), and the Key Research and Development Plan of Yunnan Province (202203AC100003).

REFERENCES CITED

- Akciz, S., Burchfiel, B.C., Crowley, J.L., Yin, J.Y., and Chen, L.Z., 2008, Geometry, kinematics, and regional significance of the Chong Shan shear zone, Eastern Himalayan Syntaxis, Yunnan, China: *Geosphere*, v. 4, no. 1, p. 292–314, <https://doi.org/10.1130/GES00111.1>.
- BGMRYP (Bureau of Geology and Mineral Resources of Yunnan Province), 1990, *Regional Geology of Yunnan Province*: Beijing, Geological Publishing House, 729 p. [in Chinese].
- Bi, L.S., 2014, Metamorphism and deformation characteristics of metamorphic rocks in Shangyun–Huimin section of Changning–Menglian suture, Yunnan, China [Master's dissertation]: Beijing, China University of Geosciences, 68 p. [in Chinese with English abstract].

- Bi, L.S., Liang, X., Wang, G.H., Zhang, H.D., Wang, Q., and Wu, C.J., 2018, Metamorphic-deformation phases and Ar–Ar chronological constraints of the Lancang Group in the middle and southern sections of the Lancangjiang Tectonic belt, western Yunnan: *Earth Science*, v. 43, no. 9, p. 3252–3266.
- Chappell, B.W., Bryant, C.J., and Wyborn, D., 2012, Per-aluminous I-type granites: *Lithos*, v. 153, p. 142–153, <https://doi.org/10.1016/j.lithos.2012.07.008>.
- Cong, F., Wu, F.Y., Li, W.C., Mou, C.L., Huang, X.M., Wang, B.D., Hu, F.Y., and Peng, Z.M., 2020, Origin of the Triassic Lincang granites in the southeastern Tibetan Plateau: Crystallization from crystal mush: *Lithos*, v. 360–361, <https://doi.org/10.1016/j.lithos.2020.105452>.
- Deng, J., Wang, Q.F., Li, G.J., Li, C.S., and Wang, C.M., 2014, Tethys tectonic evolution and its bearing on the distribution of important mineral deposits in the Sanjiang region, SW China: *Gondwana Research*, v. 26, no. 2, p. 419–437, <https://doi.org/10.1016/j.gr.2013.08.002>.
- Deng, J., Wang, C., Zi, J.W., Xia, R., and Li, Q., 2018, Constraining subduction-collision processes of the Paleo-Tethys along the Changning–Menglian suture: New zircon U–Pb ages and Sr–Nd–Pb–Hf–O isotopes of the Lincang Batholith: *Gondwana Research*, v. 62, p. 75–92, <https://doi.org/10.1016/j.gr.2017.10.008>.
- Dong, G., Mo, X., Zhao, Z., Zhu, D., Goodman, R.C., Kong, H., and Wang, S., 2013, Zircon U–Pb dating and the petrological and geochemical constraints on Lincang granite in Western Yunnan, China: Implications for the closure of the Paleo-Tethys Ocean: *Journal of Asian Earth Sciences*, v. 62, p. 282–294, <https://doi.org/10.1016/j.jseas.2012.10.003>.
- Duan, X.D., Li, J., Zeng, W.T., and Feng, W.J., 2006, The discovery of Ganlongtang tectonic melange in the middle section of Changning–Menglian zone: *Yunnan Geology*, v. 25, p. 53–62 [in Chinese with English abstract].
- Fan, W.M., Peng, T.P., and Wang, Y.J., 2009, Triassic magmatism in the southern Lancangjiang zone, southwestern China and its constraints on the tectonic evolution of Paleo-Tethys: *Earth Science Frontiers*, v. 16, p. 291–302 [in Chinese with English abstract].
- Fan, W.M., Wang, Y.J., Zhang, A.M., Zhang, F.F., and Zhang, Y.Z., 2010, Permian arc–back-arc basin development along the Ailaoshan tectonic zone: Geochemical, isotopic and geochronological evidence from the Mojiang volcanic rocks, Southwest China: *Lithos*, v. 119, no. 3–4, p. 553–568, <https://doi.org/10.1016/j.lithos.2010.08.010>.
- Fan, W.M., Wang, Y., Zhang, Y., Zhang, Y., Jourdan, F., Zi, J., and Liu, H., 2015, Paleotethyan subduction process revealed from Triassic blueschists in the Lancang tectonic belt of Southwest China: *Tectonophysics*, v. 662, p. 95–108, <https://doi.org/10.1016/j.tecto.2014.12.021>.
- Fang, N., Liu, B., Feng, Q., and Jia, J., 1994, Late Palaeo-tethys in the Changning–Menglian and Lancangjiang belts, southwestern Yunnan: *Journal of Southeast Asian Earth Sciences*, v. 9, p. 363–374, [https://doi.org/10.1016/0743-9547\(94\)90048-5](https://doi.org/10.1016/0743-9547(94)90048-5).
- Feng, Q., and Liu, B., 1993, A new Early Devonian radiolarian genus from western Yunnan: *Science in China: Series B, Earth Sciences*, v. 36, p. 242–248 [in Chinese with English abstract].
- Feng, Q.L., 2002, Stratigraphy of volcanic rocks in the Changning–Menglian Belt in southwestern Yunnan, China: *Journal of Asian Earth Sciences*, v. 20, p. 657–664, [https://doi.org/10.1016/S1367-9120\(02\)00006-8](https://doi.org/10.1016/S1367-9120(02)00006-8).
- Fu, Y.-z., et al., 2021, Petrology and metamorphism of glaucophane eclogites in Changning–Menglian suture zone, Bangbong area, southeast Tibetan Plateau: An evidence for Paleo-Tethys subduction: *China Geology*, v. 4, p. 111–125, <https://doi.org/10.31035/cg2021017>.
- Griffine, W.L., Powell, W.J., Pearson, N.J., and O'Reilly, S.Y., 2008, GLITTER: Data reduction software for laser ablation ICP-MS. Laser ablation-ICP-MS in the Earth sciences: Mineralogical Association of Canada, v. 40, p. 204–207.
- Hara, H., Ito, T., Tokiwa, T., Kong, S., and Lim, P., 2020, The origin of the Pailin crystalline complex in western Cambodia, and back-arc basin development in the Paleo Tethys Ocean: *Gondwana Research*, v. 82, p. 299–316, <https://doi.org/10.1016/j.gr.2020.01.007>.

- Harrison, T.M., Duncan, I., and McDougall, I., 1985, Diffusion of ^{40}Ar in biotite: Temperature, pressure and compositional effects: *Geochimica et Cosmochimica Acta*, v. 49, p. 2461–2468, [https://doi.org/10.1016/0016-7037\(85\)90246-7](https://doi.org/10.1016/0016-7037(85)90246-7).
- Helmcke, D., 1985, The Permo-Triassic “Paleotethys” in mainland southeast-Asia and adjacent parts of China: *Geologische Rundschau*, v. 74, p. 215–228, <https://doi.org/10.1007/BF01824893>.
- Hennig, D., Lehmann, B., Frei, D., Belyatsky, B., Zhao, X.F., Cabral, A.R., Zeng, P.S., Zhou, M.F., and Schmidt, K., 2009, Early Permian seafloor to continental arc magmatism in the eastern Paleo-Tethys: U-Pb age and Nd-Sr isotope data from the southern Lancangjiang zone, Yunnan, China: *Lithos*, v. 113, p. 408–422, <https://doi.org/10.1016/j.lithos.2009.04.031>.
- Heppe, K., Helmcke, D., and Wemmer, K., 2007, The Lancang River Zone of southwestern Yunnan, China: A questionable location for the active continental margin of Paleotethys: *Journal of Asian Earth Sciences*, v. 30, p. 706–720, <https://doi.org/10.1016/j.jseas.2007.04.002>.
- Hoskin, P.W.O., and Schaltegger, U., 2003, The composition of zircon and igneous and metamorphic petrogenesis: Reviews in Mineralogy and Geochemistry, v. 53, no. 1, p. 27–62, <https://doi.org/10.2113/0530027>.
- Hu, F., Liu, S., Ducea, M.N., Chapman, J.B., Wu, F., and Kusky, T., 2020, Early Mesozoic magmatism and tectonic evolution of the Qinling Orogen: Implications for oblique continental collision: *Gondwana Research*, v. 88, p. 296–332, <https://doi.org/10.1016/j.gr.2020.07.006>.
- Hu, F., Wu, F.Y., Wang, J.G., Ducea, M.N., Chapman, J.B., Zaw, K., Lin, W., Sein, K., and Meffre, S., 2022, Newly discovered Early Carboniferous and Late Permian magmatic rocks in eastern Myanmar: Implications for the tectonic evolution of the eastern Paleo-Tethys: *Journal of Asian Earth Sciences*, v. 227, <https://doi.org/10.1016/j.jseas.2022.105093>.
- Ito, T., Hara, H., Kong, S., and Lim, P., 2020, New materials of Cisuralian (Early Permian) radiolarians from western Cambodia: Paleobiogeographic implications in the Paleotethys: *Palaeoworld*, v. 29, p. 568–576, <https://doi.org/10.1016/j.palwor.2019.08.001>.
- Jian, P., Liu, D., and Sun, X., 2003, SHRIMP dating of Baimaxueshan and Ludian granitoid batholiths, northwestern Yunnan Province, and its geological implications: *Acta Petrologica Sinica* (Yanshi Xuebao), v. 24, p. 337–342 [in Chinese with English abstract].
- Jian, P., Liu, D., Kröner, A., Zhang, Q., Wang, Y., Sun, X., and Zhang, W., 2009a, Devonian to Permian plate tectonic cycle of the Paleo-Tethys Orogen in southwest China (I): Geochemistry of ophiolites, arc/back-arc assemblages and within-plate igneous rocks: *Lithos*, v. 113, p. 748–766, <https://doi.org/10.1016/j.lithos.2009.04.004>.
- Jian, P., Liu, D., Kröner, A., Zhang, Q., Wang, Y., Sun, X., and Zhang, W., 2009b, Devonian to Permian plate tectonic cycle of the Paleo-Tethys Orogen in southwest China (II): Insights from zircon ages of ophiolites, arc/back-arc assemblages and within-plate igneous rocks and generation of the Emeishan CFB province: *Lithos*, v. 113, p. 767–784, <https://doi.org/10.1016/j.lithos.2009.04.006>.
- Keller, C.B., Schoene, B., Barboni, M., Samperton, K.M., and Husson, J.M., 2015, Volcanic plutonic parity and the differentiation of the continental crust: *Nature*, v. 523, p. 301–307, <https://doi.org/10.1038/nature14584>.
- Kong, H.L., Dong, G.C., Mo, X.X., Zhao, Z.D., Zhu, D.C., Wang, S., Li, R., and Wang, Q.L., 2012, Petrogenesis of Lincang granites in Sanjiang area of western Yunnan Province: Constraints from geochemistry, zircon U-Pb geochronology and Hf isotope: *Acta Petrologica Sinica* (Yanshi Xuebao), v. 28, p. 1438–1452 [in Chinese with English abstract].
- Koppers, A.A.P., 2002, ArArCalc-software for $^{40}\text{Ar}/^{39}\text{Ar}$ age calculations: *Computers & Geosciences*, v. 28, no. 5, p. 605–619, [https://doi.org/10.1016/S0098-3004\(01\)00095-4](https://doi.org/10.1016/S0098-3004(01)00095-4).
- Li, G.Z., Li, C., Ripley, E.M., Kamo, S., and Su, S.G., 2012, Geochronology, petrology and geochemistry of the Nanlinshan and Banpo mafic-ultramafic intrusions: Implications for subduction initiation in the eastern Paleo-Tethys: Contributions to Mineralogy and Petrology, v. 164, no. 5, p. 773–788, <https://doi.org/10.1007/s00410-012-0770-4>.
- Li, J., Sun, Z.B., Huang, L., Xu, G.X., Tian, S.M., Deng, R.H., and Zhou, K., 2017, P-T-t path and geological significance of retrograded eclogites from Mengku area in western Yunnan Province, China: *Acta Petrologica Sinica*, v. 33, no. 7, p. 2285–2301 [in Chinese with English abstract].
- Li, W.C., Pan, G.T., Zhang, X.F., Wang, L.Q., and Zhou, J.X., 2021, Tectonic evolution and multi-episodic metallogenesis of the Sanjiang Paleo-Tethys multi-arc-basinterrane system, SW Tibetan Plateau: *Journal of Asian Earth Sciences*, v. 221, <https://doi.org/10.1016/j.jseas.2021.104932>.
- Liao, S.Y., Yin, F.G., Sun, Z.M., Wang, D.B., Tang, Y., and Sun, J., 2013, Early Middle Triassic mafic dikes from the Baoshan subterranean, western Yunnan: Implications for the tectonic evolution of the Palaeo-Tethys in Southeast Asia: *International Geology Review*, v. 55, no. 8, p. 976–993, <https://doi.org/10.1080/00206814.2012.758354>.
- Liu, C.S., Zhu, J., and Xu, X.S., 1989, Study on the characteristics of Lincang composite granite batholith in west Yunnan: *Yunnan Geology*, v. 8, no. 3–4, p. 189–204 [in Chinese].
- Ludwig, K.R., 2003, Isoplot 3.0, A Geochronological Toolkit for Excel: Berkeley Geochronology Center Special Publication 4, 70 p.
- McDougall, I., and Harrison, T.M., 1999, *Geochronology and Thermochronology by the $^{40}\text{Ar}/^{39}\text{Ar}$ Method* (2nd edition): New York, Oxford University Press, 269 p.
- Metcalfe, I., 1996, Gondwanaland dispersion, Asian accretion and evolution of eastern Tethys: *Australian Journal of Earth Sciences*, v. 43, p. 605–623, <https://doi.org/10.1080/08120099608728282>.
- Metcalfe, I., 2006, Palaeozoic and Mesozoic tectonic evolution and palaeogeography of East Asian crustal fragments: The Korean Peninsula in context: *Gondwana Research*, v. 9, p. 24–46, <https://doi.org/10.1016/j.gr.2005.04.002>.
- Metcalfe, I., 2011, Tectonic framework and Phanerozoic evolution of Sundaland: *Gondwana Research*, v. 19, p. 3–21, <https://doi.org/10.1016/j.gr.2010.02.016>.
- Metcalfe, I., 2013, Gondwana dispersion and Asian accretion: Tectonic and paleogeographic evolution of eastern Tethys: *Journal of Asian Earth Sciences*, v. 66, p. 1–33, <https://doi.org/10.1016/j.jseas.2012.12.020>.
- Metcalfe, I., 2021, Multiple Tethyan ocean basins and orogenic belts in Asia: *Gondwana Research*, v. 100, p. 87–130, <https://doi.org/10.1016/j.gr.2021.01.012>.
- Mo, X.X., Shen, S.Y., and Zhu, Q.W., 1998, Volcanic-Ophiolite and Mineralization of Middle and Southern Part in Sanjiang, Southern China: Beijing, Geological Publishing House, 128 p. [in Chinese].
- Morley, C.K., 2018, Understanding Sibumasu in the context of ribbon continents: *Gondwana Research*, v. 64, p. 184–215, <https://doi.org/10.1016/j.gr.2018.07.006>.
- Nie, X.M., Feng, Q., Qian, X., and Wang, Y.J., 2015, Magmatic record of Prototethyan evolution in SW Yunnan, China: Geochemical, zircon U-Pb geochronological and Lu-Hf isotopic evidence from the Huimin metavolcanic rocks in the southern Lancangjiang zone: *Gondwana Research*, v. 28, no. 2, p. 757–768, <https://doi.org/10.1016/j.gr.2014.05.011>.
- Nie, X.M., Feng, Q., Metcalfe, I., Baxter, A.T., and Liu, G., 2016, Discovery of a Late Devonian magmatic arc in the southern Lancangjiang zone, western Yunnan: Geochemical and zircon U-Pb geochronological constraints on the evolution of Tethyan Ocean basins in SW China: *Journal of Asian Earth Sciences*, v. 118, p. 32–50, <https://doi.org/10.1016/j.jseas.2015.12.026>.
- Peng, T.P., Wang, Y., Zhao, G., Fan, W., and Peng, B., 2008, Arc-like volcanic rocks from the southern Lancangjiang zone, SW China: Geochronological and geochemical constraints on their petrogenesis and tectonic implications: *Lithos*, v. 102, p. 358–373, <https://doi.org/10.1016/j.lithos.2007.08.012>.
- Peng, T.P., Wilde, S.A., Wang, Y.J., Fan, W.M., and Peng, B.X., 2013, Mid-Triassic felsic igneous rocks from the southern Lancangjiang zone, SW China: Petrogenesis and implications for the evolution of Paleo-Tethys: *Lithos*, v. 168–169, p. 15–32, <https://doi.org/10.1016/j.lithos.2013.01.015>.
- Qian, X., Feng, Q.L., Chonglakmani, C., and Monjai, D., 2013, Geochemical and geochronological constraints on the Chiang Khong volcanic rocks (Northwestern Thailand) and its tectonic implications: *Frontiers of Earth Science*, v. 7, p. 508–521, <https://doi.org/10.1007/s11707-013-0399-2>.
- Qian, X., Feng, Q.L., Wang, Y.J., Chonglakmani, C., and Monjai, D., 2016a, Geochronological and geochemical constraints on the mafic rocks along the Luang Prabang zone: Carboniferous back-arc setting in northwest Laos: *Lithos*, v. 245, p. 60–75, <https://doi.org/10.1016/j.lithos.2015.07.019>.
- Qian, X., Feng, Q.L., Wang, Y.J., Yang, W.Q., Chonglakmani, C., and Monjai, D., 2016b, Petrochemistry and tectonic setting of the Middle Triassic arc-like volcanic rocks in the Sayabouli area, NW Laos: *Journal of Earth Science*, v. 27, p. 365–377, <https://doi.org/10.1007/s12583-016-0669-5>.
- Qiu, H.N., and Wijbrans, J.R., 2008, The Paleozoic metamorphic history of the central orogenic belt of China from $^{40}\text{Ar}/^{39}\text{Ar}$ geochronology of eclogite garnet fluid inclusions: *Earth and Planetary Science Letters*, v. 268, no. 3–4, p. 501–514, <https://doi.org/10.1016/j.epsl.2008.01.042>.
- Sone, M., Metcalfe, I., and Chaodumrong, P., 2012, The Chanthaburi terrane of southeastern Thailand: Stratigraphic confirmation as a disrupted segment of the Sukhothai Arc: *Journal of Asian Earth Sciences*, v. 61, p. 16–32, <https://doi.org/10.1016/j.jseas.2012.08.021>.
- Stipp, M., Stünitz, H., Heilbronner, R., and Schmid, S.M., 2002, The eastern Tonalite fault zone: A ‘natural laboratory’ for crystal plastic deformation of quartz over a temperature range from 250 to 700°C: *Journal of Structural Geology*, v. 24, p. 1861–1884, [https://doi.org/10.1016/S0191-8141\(02\)00035-4](https://doi.org/10.1016/S0191-8141(02)00035-4).
- Sun, Z.B., Li, J., Zhou, K., Zeng, W.T., Duan, X.D., Zhao, J.T., Xu, G.X., and Fan, Y.H., 2017, Geochemical characteristics and geological significance of retrograde eclogite in Mengku area, Shuangjiang County, Western Yunnan Province: China: *Geoscience*, v. 31, no. 4, p. 746–756 [in Chinese with English abstract].
- Sun, Z.B., Hu, S.B., Zhao, F., Li, X.J., Bao, J.F., Zhang, X.F., and She, Z.M., 2020, Petrogenesis and tectonic implication of Manjing granitoids, Southern Lancangjiang zone: Constraints by geochemistry, zircon U-Pb chronology and Hf isotope: *Acta Petrologica Sinica* (Yanshi Xuebao), v. 36, no. 5, p. 1389–1408, <https://doi.org/10.18654/1000-0569/2020.05.05>.
- Ueno, K., 1999, Gondwana/Tethys divide in East Asia, solution from late Paleozoic foraminiferal paleobiogeography, in Ratanasthien, B., and Riebel, S.L., eds., *Proceedings of the International Symposium on Shallow Tethys 5: Chiang Mai, Thailand*, Department of Geological Science, Faculty of Science, Chiang Mai University, p. 45–54.
- Ueno, K., and Hisada, K., 1999, Closure of the Paleo-Tethys caused by the collision of Indochina and Sibumasu: *Chikyu Monthly*, v. 21, p. 832–839 [in Japanese].
- Ueno, K., and Hisada, K., 2001, The Nan-Uttaradit-Sa Kao Suture as a main Paleo-Tethys suture in Thailand: Is it real? *Gondwana Research*, v. 4, p. 804–806, [https://doi.org/10.1016/S1342-937X\(05\)70590-6](https://doi.org/10.1016/S1342-937X(05)70590-6).
- Van Acherbergh, E., Ryan, C.G., and Griffin, W.L., 1999, GLITTER: On-line interactive data reduction for the laser ablation inductively coupled plasma mass spectrometry microprobe, in *Ninth Annual V.M. Goldschmidt Conference*: Cambridge, Massachusetts, Harvard University Department of Earth and Planetary Sciences, p. 7215.
- Wan, B., Wu, F.Y., Chen, L., Zhao, L., Liao, X.F., Xiao, W.J., and Zhu, R.X., 2019, Cyclical one way continental rupture-drift in the Tethyan evolution: Subduction-driven plate tectonics: *Science China: Earth Sciences*, v. 62, no. 12, p. 2005–2016, <https://doi.org/10.1007/s11430-019-9393-4>.
- Wang, B.D., Wang, L.Q., Pan, G.T., Yin, F.G., Wang, D.B., and Tang, Y., 2013, U-Pb zircon dating of Early Paleozoic gabbro from the Nantinghe ophiolite in the Changning-Menglian suture zone and its geological implication: *Chinese Science Bulletin*, v. 58, no. 8, p. 920–930, <https://doi.org/10.1007/s11434-012-5481-8>.

- Wang, B.D., Wang, L.Q., Chen, J.L., Yin, F.G., Wang, D.B., Zhang, W.P., Chen, L.K., and Liu, H., 2014a, Triassic three-stage collision in the Paleo-Tethys: Constraints from magmatism in the Jiangda-Deqen-Weixi continental margin arc, SW China: *Gondwana Research*, v. 26, p. 475–491, <https://doi.org/10.1016/j.gr.2013.07.023>.
- Wang, B.D., Wang, L.Q., Wang, D.B., Yin, F.G., He, J., Peng, Z.M., and Yan, G.C., 2018a, Tectonic evolution of the Changning-Menglian proto-paleo Tethys Ocean in the Sanjiang area, Southwestern China: *Earth Science*, v. 43, no. 8, p. 2527–2550.
- Wang, C.M., Deng, J., Santosh, M., McCuaig, T.C., Lu, Y.J., Carranza, E.J.M., and Wang, Q.F., 2015, Age and origin of the Bulangshan and Mengsong granitoids and their significance for post-collisional tectonics in the Changning-Menglian Paleo-Tethys Orogen: *Journal of Asian Earth Sciences*, v. 113, p. 656–676, <https://doi.org/10.1016/j.jseas.2015.05.001>.
- Wang, D.B., Luo, L., Tang, Y., Yin, F.G., Wang, B.D., and Wang, L.Q., 2016a, Zircon U-Pb dating and petrogenesis of early Paleozoic adakites from the Niujiangshan ophiolitic mélange in the Changning-Menglian suture zone and its geological implications: *Acta Petrologica Sinica* (Yanshi Xuebao), v. 32, no. 8, p. 2317–2329.
- Wang, F., Liu, F.L., Liu, P.H., Shi, J.R., and Cai, J., 2014b, Petrogenesis of Lincang granites in the south of Lancangjiang area: Constrain from geochemistry and zircon U-Pb geochronology: *Acta Petrologica Sinica*, v. 30, no. 10, p. 3034–3050 [in Chinese with English abstract].
- Wang, F., Liu, F., Schertl, H.-P., Liu, P., Ji, L., Cai, J., and Liu, L., 2019, Paleo-Tethys tectonic evolution of Lancangjiang metamorphic complex: Evidence from SHRIMP U-Pb zircon dating and $^{40}\text{Ar}/^{39}\text{Ar}$ isotope geochronology of blueschists in Xiaohaijiang-Xiayun area, Southeastern Tibetan Plateau: *Gondwana Research*, v. 65, p. 142–155, <https://doi.org/10.1016/j.gr.2018.08.007>.
- Wang, H.N., Liu, F., Santosh, M., and Wang, F., 2020a, Subduction erosion associated with Paleo-Tethys closure: Deep subduction of sediments and high pressure metamorphism in the SE Tibetan Plateau: *Gondwana Research*, v. 82, p. 171–192, <https://doi.org/10.1016/j.gr.2020.01.001>.
- Wang, H.N., Liu, F., Sun, Z., Ji, L., Cai, J., and Zhu, J., 2021, Identification of continental-type eclogites in the Paleo-Tethys Changning-Menglian orogenic belt, southeastern Tibetan Plateau: Implications for the transition from oceanic to continental subduction: *Lithos*, v. 396–397, <https://doi.org/10.1016/j.lithos.2021.106215>.
- Wang, S., Dong, G.C., Mo, X.X., Zhao, Z.D., Zhu, D.C., Kong, H.L., Wang, X., and Nie, F., 2012, Petrological and geochemical characteristics, Ar-Ar geochronology study and their tectonic significance of Triassic volcanic rocks in southern Lancangjiang zone: *Acta Petrologica Sinica* (Yanshi Xuebao), v. 28, no. 4, p. 1148–1162.
- Wang, Y., Schoenbohm, L.M., Zhang, B., Granger, D.E., Zhou, R., Zhang, J., and Hou, J., 2017, Late Cenozoic landscape evolution along the Ailao Shan Shear Zone, SE Tibetan Plateau: Evidence from fluvial longitudinal profiles and cosmogenic erosion rates: *Earth and Planetary Science Letters*, v. 472, p. 323–333, <https://doi.org/10.1016/j.epsl.2017.05.030>.
- Wang, Y., Wang, Y.J., Zhang, P., Lindsay, M.S., Zhang, B., Zhang, J., Zhou, R., Daniel, F.S., Erin, G.S., Wang, F., and Liu, W., 2020b, Intracontinental deformation within the India-Eurasia oblique convergence zone: Case studies on the Nantinghe and Dayingjiang faults: *Geological Society of America Bulletin*, v. 132, p. 850–862, <https://doi.org/10.1130/B35338.1>.
- Wang, Y., Wang, Y.J., Zhang, P., Zhang, J., Zhang, B., Zhang, Y., Zhou, R., Seagren, E.G., Qian, X., and Li, Z., 2022, Kinematics and $^{40}\text{Ar}/^{39}\text{Ar}$ geochronology of the Lincang-Inthanon tectonic belt: Implication for Cenozoic tectonic extrusion of SE Asia: *Geological Society of America Bulletin*, v. 134, p. 2854–2866, <https://doi.org/10.1130/B36187.1>.
- Wang, Y.J., Zhang, A., Fan, W., Peng, T., Zhang, F., Zhang, Y., and Bi, X., 2010, Petrogenesis of late Triassic post-collisional basaltic rocks of the Lancangjiang tectonic zone, southwest China, and tectonic implications for the evolution of the eastern Paleotethys: *Geochronological and geochemical constraints: Lithos*, v. 120, p. 529–546, <https://doi.org/10.1016/j.lithos.2010.09.012>.
- Wang, Y.J., He, H.Y., Cawood, P.A., Srithai, B., Feng, Q.L., Fan, W.M., Zhang, Y.Z., and Qian, X., 2016b, Geochronological, elemental and Sr-Nd-Hf-O isotopic constraints on the petrogenesis of the Triassic post-collisional granitic rocks in NW Thailand and its Paleotethyan implications: *Lithos*, v. 266–267, p. 264–286, <https://doi.org/10.1016/j.lithos.2016.09.012>.
- Wang, Y.J., Qian, X., Cawood, P.A., Liu, H., Feng, Q., Zhao, G., Zhang, Y., He, H., and Zhang, P., 2018b, Closure of the East Paleotethyan Ocean and amalgamation of the Eastern Cimmerian and Southeast Asia continental fragments: *Earth-Science Reviews*, v. 186, p. 195–230, <https://doi.org/10.1016/j.earscirev.2017.09.013>.
- Wang, Y.J., Yang, T.X., Zhang, Y.Z., Qian, X., Gan, C.S., Wang, Y.K., Wang, Y., and Senebottalath, V., 2020c, Late Paleozoic back-arc basin in the Indochina block: Constraints from the mafic rocks in the Nan and Luang Prabang tectonic zones, Southeast Asia: *Journal of Asian Earth Sciences*, v. 195, p. 1–20, <https://doi.org/10.1016/j.jseas.2020.104333>.
- Wei, C., Qi, X.X., Chang, Y.L., Ji, F.B., and Zhang, S.Q., 2016, Identification on age of Xiaodingxi Formation volcanic rocks in central-southern Lancangjiang Orogeny and its tectonic implication: *Acta Geologica Sinica*, v. 90, no. 11, p. 3192–3214 [in Chinese with English abstract].
- Wei, Y., Zi, J.-W., Liu, G., Sun, Z., Chen, G., Zhao, T., Nie, X., and Yang, Z., 2022, Reconstructing the Lancang Terrane (SW Yunnan) and implications for early Paleozoic Proto-Tethys evolution at the northern margin of Gondwana: *Gondwana Research*, v. 101, p. 278–294, <https://doi.org/10.1016/j.gr.2021.08.009>.
- Xu, Z.Q., Dilek, Y., Cao, H., Yang, J.S., Robinson, P., Ma, C.Q., Li, H.Q., Jolivet, M., Roger, F., and Chen, X.J., 2015, Paleo-Tethys evolution of Tibet as recorded in the East Cimmerides and West Cathaysides: *Journal of Asian Earth Sciences*, v. 105, p. 320–337, <https://doi.org/10.1016/j.jseas.2015.01.021>.
- Yan, G., Wang, B., Liu, H., and Wu, Z., 2022, Geochronology and geochemistry of the Manxin ophiolitic mélange in the Changning-Menglian Suture Zone, southwest China: Implications for the tectonic evolution of the Proto-Tethys Ocean: *Geological Journal*, v. 58, p. 921–1323.
- Zhai, Q.G., Chung, S.L., Tang, Y., Hu, P.Y., Jin, X.C., Wang, J., Wang, H.T., Wang, K.L., and Lee, H.Y., 2019, Late Carboniferous ophiolites from the southern Lancangjiang belt, SW China: Implication for the arc-back-arc system in the eastern Paleo-Tethys: *Lithos*, v. 344–345, p. 134–146, <https://doi.org/10.1016/j.lithos.2019.06.020>.
- Zhang, B., Yin, C.Y., Zhang, J.J., Wang, J.M., Zhong, D.L., Wang, Y., Lai, Q.Z., Yue, Y.H., and Zhou, Q.Y., 2017, Midcrustal shearing and doming in a Cenozoic compressive setting along the Ailao Shan-Red River shear zone: *Geochemistry, Geophysics, Geosystems*, v. 18, p. 400–433, <https://doi.org/10.1002/2016GC006520>.
- Zhang, Q., Wang, C.Y., Liu, D., Jian, P., Qian, Q., Zhou, G.Q., and Robinson, P.T., 2008, A brief review of ophiolites in China: *Journal of Asian Earth Sciences*, v. 32, no. 5–6, p. 308–324, <https://doi.org/10.1016/j.jseas.2007.11.012>.
- Zhao, F., Li, G.J., Zhang, P.F., Wang, C.B., Sun, Z.B., and Tang, X., 2018, Petrogenesis and tectonic implications of the Lincang batholith in the Sanjiang, Southwest China: Constraints by geochemistry, zircon U-Pb chronology and Hf isotope: *Acta Petrologica Sinica*, v. 34, no. 5, p. 1397–1412 [in Chinese with English abstract].
- Zhao, J., Zhong, D.L., and Wang, Y., 1994, Metamorphism of Lancang metamorphic belt, the western Yunnan and its relation to deformation: *Acta Petrologica Sinica* (Yanshi Xuebao), v. 10, p. 27–40 [in Chinese with English abstract].
- Zhong, D.L., 1998, Paleo-Tethys Orogen in Western Yunnan and Sichuan Provinces: Beijing, Science Press.
- Zhu, W.G., Zhong, H., Wang, L.Q., He, D.F., Ren, T., Fan, H.P., and Bai, Z.J., 2011, Petrogenesis of the basalts and rhyolite porphyries of the Minle copper deposit, Yunnan: Geochronological and geochemical constraints: *Acta Petrologica Sinica* (Yanshi Xuebao), v. 27, p. 2694–2708 [in Chinese with English abstract].

SCIENCE EDITOR: WENJIAO XIAO

ASSOCIATE EDITOR: YONGJIANG LIU

MANUSCRIPT RECEIVED 24 OCTOBER 2022

REVISED MANUSCRIPT RECEIVED 4 APRIL 2023

MANUSCRIPT ACCEPTED 7 MAY 2023

Printed in the USA